DOE/NASA/51040-53
NASA TM-83609

Oxidation and Corrosion Resistance of Candidate Stirling Engine Heater-Head-Tube Alloys

Joseph R. Stephens and Charles A. Barrett
National Aeronautics and Space Administration
Lewis Research Center

May 1984

Prepared for
U.S. DEPARTMENT OF ENERGY
Conservation and Renewable Energy
Office of Vehicle and Engine R&D

DOE/NASA/51040-53
NASA TM-83609

Oxidation and Corrosion Resistance of Candidate Stirling Engine Heater-Head-Tube Alloys

Joseph R. Stephens and Charles A. Barrett
National Aeronautics and Space Administration
Lewis Research Center
Cleveland, Ohio 44135

May 1984

Work performed for
U.S. DEPARTMENT OF ENERGY
Conservation and Renewable Energy
Office of Vehicle and Engine R&D
Washington, D.C. 20545
Under Interagency Agreement DE-AI01-77CS51040

DISCLAIMER

Printed in the United States of America

Available from
National Technical Information Service
U.S. Department of Commerce
5285 Port Royal Road
Springfield, VA 22161

NTIS price codes[1]
Printed copy: A03
Microfiche copy: A01

[1]Codes are used for pricing all publications. The code is determined by the number of pages in the publication. Information pertaining to the pricing codes can be found in the current issues of the following publications, which are generally available in most libraries: *Energy Research Abstracts (ERA); Government Reports Announcements* and Index (*GRA* and I); *Scientific and Technical Abstract Reports (STAR);* and publication, NTIS-PR-360 available from NTIS at the above address.

Summary

An experimental investigation was undertaken to determine the oxidation and corrosion resistance of candidate Stirling engine heater-head-tube alloys under conditions simulating automotive applications of the Stirling engine. Duplicate sheet specimens of 16 alloys were evaluated for 3500 hr under cyclic conditions at 820° C in a Stirling engine simulator materials test rig. The specimens were heated for 5-hr cycles in the combustion flame of the diesel-fuel-fired rig. Specific weight change data fitted to an attack parameter equation were used to quantify the environmental resistance of the alloys. X-ray diffraction, metallographic, and electron microprobe analyses were used to supplement the weight change data analyses.

Ten of the alloys exhibited excellent or good environmental resistance; the remaining six alloys had only poor or catastrophic resistance. Three of the alloys, CG-27, Sanicro 32, and 12RN72, were judged to be leading candidate heater-head-tube alloys. On the basis of other considerations such as low strength, high cost, and high strategic metal content the remaining seven alloys with excellent or good environmental resistance were given much lower priority. Alloy CG-27 was given the highest priority. The strengths of Sanicro 32 and 12RN72 are in question at the high operating temperatures, 820° to 870° C, of current designs for the automotive Stirling engine. Electron microprobe analysis of the oxide scales formed on CG-27 indicated an outer surface oxide rich in iron, nickel, and aluminum; an intermediate oxide scale rich in chromium and titanium; and an aluminum-rich subscale adjacent to the metal. Beneath the oxide layers was a zone of alloy substrate that exhibited internal oxidation, primarily of aluminum along with some titanium. Of the alloys investigated, CG-27 contains the least amount of the strategic metal chromium (13 percent) and none of the strategic metal cobalt. Alloy N-155, used in current prototype engines, contains 20 percent chromium and 20 percent cobalt.

Introduction

The Department of Energy (DOE) and NASA (ref. 1) are currently investigating the Stirling engine as an alternative power source to the internal combustion engine for automotive applications. The Stirling engine (fig. 1) is an externally heated engine that offers the advantages of high efficiency, low pollution, low noise, and multifuel capability. Hydrogen is used as the working fluid for automotive applications in order to obtain maximum efficiency from the engine. Heat is input to the working fluid by a combustion flame impinging on the outside walls of the tubes containing the hydrogen working fluid. Current engines designed for automotive applications use tubes with a wall thickness of 0.75 mm (3.0 mm i.d. by 4.5 mm o.d.). The thin wall is required to achieve maximum heat input to the hydrogen. However, the tube material must be of sufficient strength to contain the hydrogen, which operates at high pressures and temperatures. Automotive design requirements call for a normal maximum pressure of 15 MPa, with peak pressures reaching 21 MPa during transient conditions. Tube walls are designed for an average temperature of 820° C, with 870° C common on the flame side. A further requirement is that the tubes operate for a period of 3500 hr, which is approximately equivalent to the 160 000-km (100 000-mile) driving life of an engine.

The tubes currently are heated by direct exposure to a combustion flame fired by gasoline or diesel fuel. Alternative fuels such as alcohol and shale oil derivatives may be considered for future applications. Oxidation and corrosion resistance is a primary criterion for selecting heater-head-tube alloys to withstand the extreme operating requirements of the Stirling engine.

Excessive scale spalling will reduce the tube wall thickness and lead to premature failure caused by the high-pressure hydrogen rupturing the tubes or permeating rapidly through the tube walls. Prototype engines and initial models of experimental automotive engines use N-155 (Multimet) for heater head tubes. However, this iron-base alloy contains 20 percent cobalt, a costly and strategic metal. Efforts are currently under way by NASA (refs. 2 to 7) and the contractors on this program, Mechanical Technology Inc. (MTI) and United Stirling Sweden (USAB), to identify substitutes for N-155. The primary emphasis is on high-strength austenitic iron-base alloys although a limited number of nickel-base superalloys are under consideration. As part of the evaluation of candidate substitute alloys the oxidation and corrosion resistance has been determined for 16 alloys.

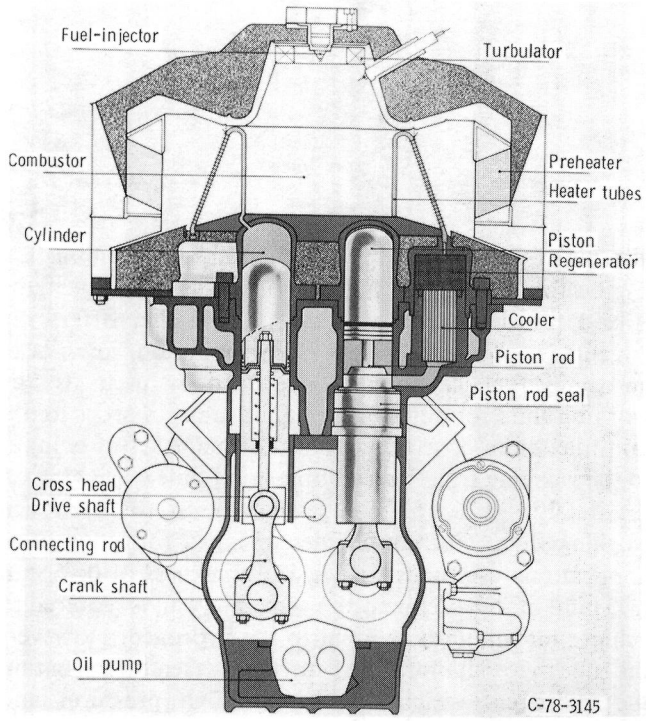

Figure 1. – Schematic representation of automotive Stirling engine.

This report describes results of oxidation and corrosion testing of the candidate heater-head-tube alloys. Flat sheet specimens were tested for 3500 hr in an environment and under cyclic temperature conditions simulating actual engine operation. In addition, specimens were tested under cyclic conditions in static air for a shorter time. The oxidation and corrosion resistance of candidate alloys was determined primarily by specific-weight-change-versus-time-data fitted to a paralinear attack parameter. X-Ray diffraction, metallographic, and electron microprobe analyses supplemented the weight change data.

Materials, Apparatus, and Experimental Procedure

Materials

Sixteen alloys (14 iron base, one nickel base, and one cobalt base) were evaluated for their oxidation and corrosion resistance under conditions of temperature and environment anticipated for automotive Stirling engines. The chemical compositions of the alloys are listed in table I. All of the alloys are commerically available except AL-EX-20, an experimental alloy supplied by Allegheny Ludlum Steel Company. Iron-base alloys are the primary candidates for automotive Stirling engine applications because their raw material costs are lower than those for nickel-base and cobalt-base alloys. Nickel-base alloys are considered as possible candidates in the event a less expensive iron-base alloy cannot be identified that will meet all of the requirements of the Stirling engine. Cobalt-base alloys are not under consideration for automotive Stirling engine applications because of the high cost of cobalt, its limited availability, and its status as a strategic material (more than 95 percent of the cobalt used in the United States is imported). However, one cobalt-base alloy (HS-188) was included in this investigation as a comparison with the iron- and nickel-base alloys.

Test coupons 1.27 cm by 2.54 cm, and generally 0.8 to 1.6 mm thick, with a 0.3-cm-diameter hanger hole, were cut from alloy sheet material. Before testing, the specimens were degreased and ultrasonically cleaned, measured with a micrometer to the nearest 0.001 mm, and weighed to the nearest 0.1 mg.

Stirling Engine Simulator Materials Test Rig

The Stirling engine simulator rig used in this program was designed and fabricated at the NASA Lewis Research Center; it consists primarily of a combustion gas heating chamber (fig. 2) with auxiliary heating, control, and gas management systems. The rig and its operation are described in detail in reference 3. The rig was fired with natural gas for initial ignition and then with diesel fuel throughout the test run. Duplicate oxidation-corrosion test specimens of the 16 alloys were suspended by platinum wires from the hairpin turns of the tubes shown in figure 2. The specimens were heated to the desired 820° C test temperature (automotive Stirling engine temperature) by the combustion flame flowing over them. The rig was used primarily as a means of ranking candidate heater-head-tube alloys (refs. 3 and 6). The oxidation-corrosion testing was conducted simultaneously with a 3500-hr endurance run of tubing alloys.

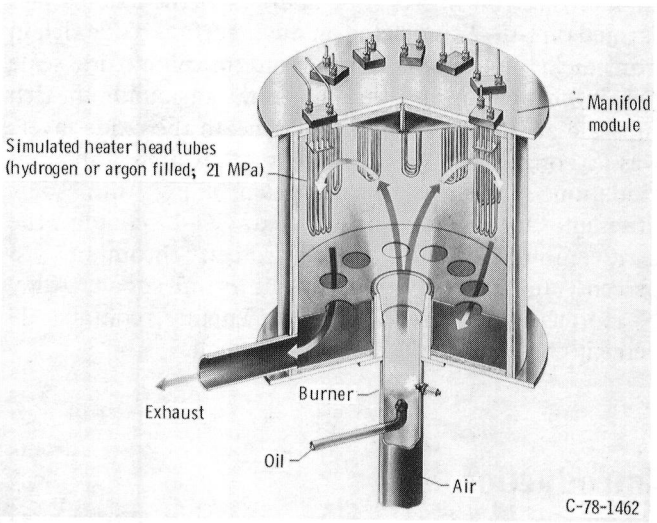

Figure 2. – Schematic representation of Stirling engine materials simulator test rig.

TABLE I. – CHEMICAL COMPOSITION OF COMMERCIAL ALLOYS

Alloy	Composition, wt %												
	Fe	Cr	Ni	Co	Mn	Si	Mo	Nb	W	Al	Ti	C	Other
Iron-base alloys													
N-155	30	21	20	20	1.5	0.5	3.0	1.0	2.5	---	---	0.15	0.15N
CG-27	38	13	38	--	.1	.1	5.5	.6	---	1.5	2.5	.05	.01B
RA-330	43	19	35	--	1.5	1.3	---	---	---	---	---	.05	-----
Sanicro 32	43	21	31	--	.6	.47	---	---	2.8	.4	.4	.89	-----
Sanicro 31H	46	21	31	--	.6	.55	---	---	---	.4	.5	.07	.02N
Incoloy 800	46	21	32	--	.75	.5	---	---	---	.38	.38	.05	-----
12RN72	47	19	30	--	1.7	.28	1.4	---	---	---	.5	.1	.02N
A-286	53	15	26	--	1.4	.4	1.25	---	---	.2	2.15	.05	.26V
W-545	54	14	26	--	1.5	.4	1.5	---	---	.2	2.85	.08	.08B
Nitronic 40	64	21	6.5	--	9.0	---	---	---	---	---	---	.04	.30N
253 MA	66	21	11	--	.4	1.7	.04	---	---	---	---	.09	.2N
316 Stainless steel	66	18	13	--	2.0	1.0	2.5	---	---	---	---	.08	-----
19-9DL	67	19	9	--	1.1	.6	1.2	.4	1.2	---	.3	.3	-----
AL-EX-20	70	5	1.0	--	20	.42	---	---	---	3.15	---	.02	-----
Nickel-base alloys													
Inconel 625[a]	3	22	61	--	0.15	0.3	9.0	4.0	---	0.2	0.2	0.05	-----
Inconel 601[a]	14	23	60	--	.5	.2	---	---	---	1.4	---	.05	-----
Inconel 718	18	18	53	--	.2	.3	3.1	5.0	---	.4	.9	.04	-----
Cobalt-base alloys													
HS-188	1.5	22	22	40	---	---	---	---	14	---	---	0.08	0.08La

[a]Evaluated in static air testing only.

An endurance run consisted of a series of 5-hr cycles to obtain the required 3500 hr of test time to simulate the minimum life of an automotive engine. A typical heating cycle consisted of a 6- to 10-minute preheat to get to the operating temperature, a 5-hr hold at temperature, and a 1-hr cooldown to near room temperature. Specimens were removed from the heating chamber at 105, 210, 420, 825, 1025, 1530, 1925, 2425, 3030, and 3500 hr and weighed to generate a weight-change-against-time curve.

Static-Air Furnace

Using duplicate test specimens, we evaluated a second series of 18 alloys (including two additional nickel-base alloys listed in table I) in a static-air furnace at 870° C, the maximum temperature anticipated for the heater head tubes. This test provided a quicker means of ranking candidate alloys and also provided a comparison with the rig data. A typical heating cycle consisted of a 2-min preheat to the operating temperature, a 1-hr hold, and a cooldown of at least 20 min to room temperature. The specimens were suspended in the individual ceramic tubes of a vertical-tube furnace. Six 2.86-cm-diameter alumina tubes were symmetrically arranged around the circumference of a 12.7-cm-diameter Kanthal A ribbon heating unit. The bottoms of the tubes were closed except for one of the tubes in which a platinum/platinum-13 percent rhodium thermocouple was exposed adjacent to the specimen. In this test setup the air was essentially static.

The specimens were automatically raised and lowered by pneumatic cylinders controlled by reset timers (fig. 3). As the specimens were raised, they were individually shielded to prevent cross spall and the six cups automatically slid under the samples to catch the oxide that spalled on cooling. This sequence occurred in roughly 10 sec. The amount of cross spall was usually low because the samples were almost completely enclosed as they cooled and the spall for each sample was trapped in its own metal foil cup.

The specimens were removed and weighed at 1, 15, 30, 45, 60, 75, 90, 100, 115, 130, 145, 160, 175, 190, and 200 hr to generate specific-weight-change-versus-time plots. The test procedure is described in detail in reference 8.

Postoxidation Procedure

After each of the two types of test the oxide retained on the specimen and its spall (available in air tests only) were analyzed by X-ray diffraction (XRD). The specimens were then sectioned horizontally across their centers and

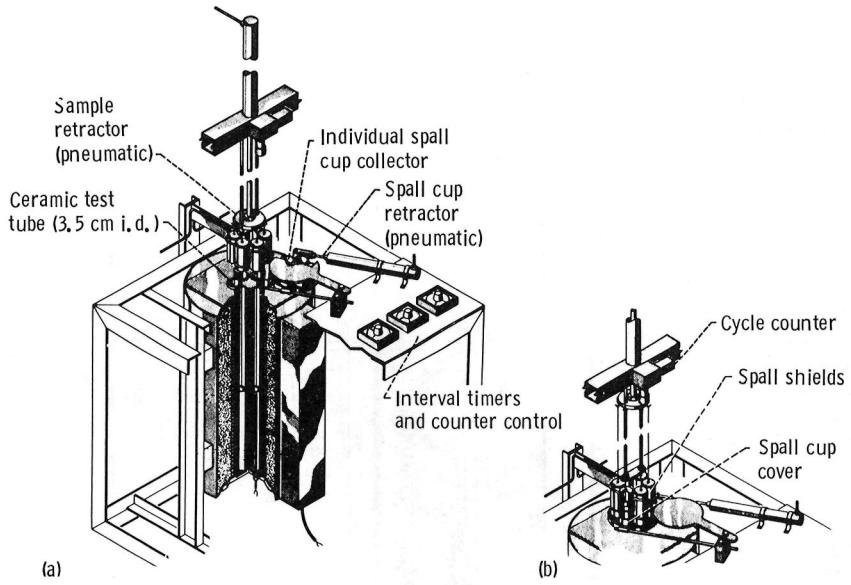

(a) Samples at test temperature.
(b) Samples cooled to ambient temperature.

Figure 3. – Multitube automatic high-temperature static-air furnace cyclic oxidation test apparatus.

mounted to determine their thicknesses metallographically. The thickness change is the difference between the initial preexposure measurement by a micrometer at the center of a sample and the postexposure metallographic thickness. The cross section was photographed at magnifications of 35, 50, or 100. A millimeter filar grid at the same magnification was also photographed and used in measuring the photomicrograph to correct for optical distortion. It is estimated that, because of variability in the sample thickness and errors in measurement, the thickness change was determined to within ±0.015 mm.

The specimen weight data were used to calculate specific specimen weight change data as a function of time for each alloy. The procedure used to analyze the specific specimen weight change data involved the method of multiple linear regression. The change in specific weight $\Delta W/A$ with time t was fitted by least squares (ref. 8) to equation (1).

$$\frac{\Delta W}{A} = k_1^{1/2} t^{1/2} - k_2 t \pm \text{SEE} \tag{1}$$

where k_1 is an oxide growth constant comparable to a parabolic oxidation scaling constant, k_2 is an oxide spalling constant, and SEE is the standard error of estimate.

An oxidation attack parameter K_a (ref. 8) was derived from equation (1) and is defined as

$$K_a = k_1^{1/2} + 10k_2 \tag{2}$$

In certain cases where scale spalling is insignificant, the k_2 term will drop out of equation (2), giving the pure parabolic oxidation and corrosion case with $k_2 = 0$. Conversely, when spalling begins very early in the test, the $k_1^{1/2}$ term will tend to drop out. In this case, K_a, defined as $20k_2t$, is a satisfactory estimate (ref. 9).

Selected alloys were examined by electron microprobe techniques to further characterize the oxidation and corrosion process occurring in the diesel-fuel-fired Stirling engine materials simulator rig. The surface of each specimen was coated with copper before metallographic mounting to prevent the electron beam from striking the plastic mounting material. Specimens were analyzed for the major alloying elements in each alloy and for oxygen.

Results

Stirling Engine Simulator Oxidation and Corrosion Tests

Weight change. – Duplicate specimens of 16 alloys were tested at 820° C for nominally 3500 hr. The test consisted of 5-hr heating cycles. Specimens were removed and weighed approximately 11 times during the run. The final $\Delta W/A$ values for the 16 alloys are listed in order of largest final weight gain to largest final weight loss (table II). The alloys could be categorized into four groups on the basis of specific weight change data. Alloys in group I had excellent oxidation and corrosion resistance, and their specific weight change was positive (weight gain) throughout the 3500-hr test. Group I comprised the five

alloys CG-27, Incoloy 800, HS-188, N-155, and Inconel 718. Three of the alloys, CG-27, Incoloy 800, and HS-188, did not exhibit any significant spalling during testing in the Stirling engine simulator rig. Final average specific weight change (fig. 4) ranged from 1.4 to 0.17 mg/cm^2 for CG-27 to Inconel 718, respectively.

A second group of alloys is considered to have relatively good oxidation and corrosion resistance under simulated Stirling engine operating conditions. The five alloys in group II in order of increasing final weight loss are RA-330, Sanicro 31H, Sanicro 32, 12RN72, and 253 MA. Final average specific weight change (fig. 5) ranged from -0.54 to -6.0 mg/cm^2 for RA-330 to 253 MA, respectively.

The third group of alloys, 316 stainless steel, W-545, A-286, and Nitronic 40 is considered to have fair to poor oxidation and corrosion resistance on the basis of specific-weight-change-versus-time data. Final average specific weight change (fig. 6) ranged from -22.8 to -41.8 mg/cm^2 for 316 stainless steel to Nitronic 40, respectively.

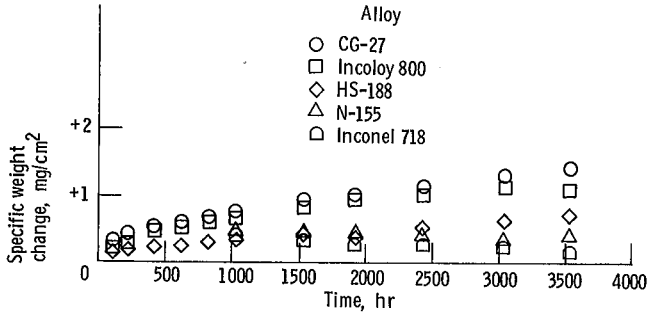

Figure 4. – Specific weight change data for group I alloys tested at 820° C for 3500 hr.

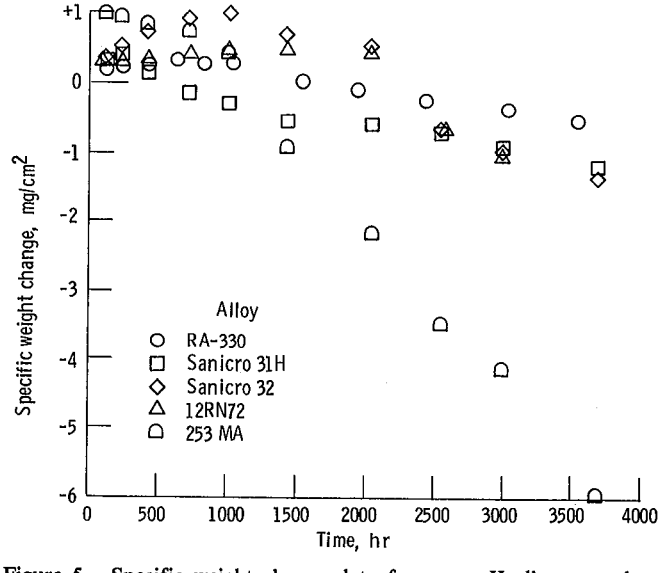

Figure 5. – Specific weight change data for group II alloys tested at 820° C for 3500 hr.

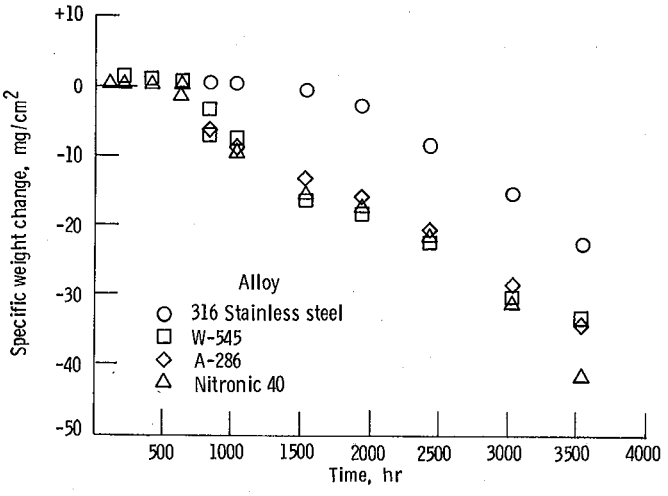

Figure 6. – Specific weight change data for group III alloys tested at 820° C for 3500 hr.

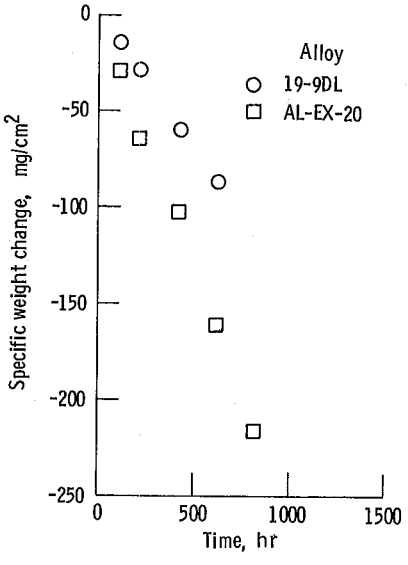

Figure 7. – Specific weight change data for group IV alloys tested at 820° C for 825 hr or less.

A final group of alloys, consisting of 19-9DL and AL-EX-20, exhibited catastrophic oxidation and corrosion behavior upon rig testing. Data for the group IV alloys are shown in figure 7. Spalling began after only a very short time into the test and excessive weight loss occurred after 500 hr of cyclic testing. The tests were terminated before the 3500-hr goal because of the unacceptable oxidation and corrosion resistance of these alloys.

Attack parameter K_a.—Oxidation and corrosion weight-change-versus-time data were fitted to the paralinear equation (eq. (1)). For three of the alloys, HS-188, Incoloy 800, and CG-27, where no spalling was observed, the attack parameter was calculated from equation (2) with $k_2 = 0$. The remaining 13 alloys also derived their attack parameters from equation (2) but

with values of k_2 included. For alloys 19-9DL, Nitronic 40, and AL-EX-20 the $k_1^{1/2}$ term dropped out so that $K_a = 20k_2t$ was used. Figure 8 is a summary plot of calculated K_a values for the 16 alloys. Values of K_a are plotted on a log scale in decreasing order of oxidation and corrosion resistance based on the highest values of the duplicate specimens. The attack parameter ranged from 0.011 for HS-188 to 12.49 for 19-9DL, or over three orders of magnitude. Examination of the K_a values in figure 8 suggested that the alloys could again be categorized into four groups. Group I comprised the alloys HS-188, Sanicro 31H, Inconel 718, Incoloy 800, N-155, CG-27, and RA-330, with K_a ranging from 0.011 for HS-188 to 0.031 for RA-330. Group II comprised the three alloys Sanicro 32, 12RN72, and 253 MA, with K_a values of 0.098, 0.110, and 0.159, respectively. Group III comprised the alloys A-286, W-545, 316 stainless steel, and Nitronic 40, with K_a ranging from 0.370 to 0.659. Group IV comprised AL-EX-20, with a K_a of 4.68, and 19-9DL, with a K_a of 12.49. This grouping was somewhat arbitrary, but corresponded to the previous grouping based on final weight change. The only exception was for RA-330, which experienced a net weight loss and was placed in group II (fig. 5) but has a K_a value similar to those for the other five alloys in group I.

Thickness change.—The thickness changes after rig testing are also listed in table II and plotted as bar graphs in figure 9. In most cases two values are noted for the total thickness change: one for general external scale formation and one for grain boundary penetration (or possibly internal oxidation), noted as internal depletion. Only HS-188 did not show evidence of a thickness change after the 3500-hr test. Two alloys, 19-9DL and AL-EX-20, exhibited extreme external scale formation, but with no detectable internal depletion. In general, high values of thickness change meant high K_a values. Since not all of the alloys achieved a 3500-hr life, a direct comparison is not possible. Therefore the rank based on alloy thickness change was plotted against the ranking based on K_a value (fig. 10). The ranking correlation coefficient ρ is a significant 0.691.

X-ray diffraction.—The X-ray diffraction data from the specimen surface after testing are summarized in table III by rank of the alloy in decreasing X-ray intensity. In general, the most oxidation and corrosion resistant alloys

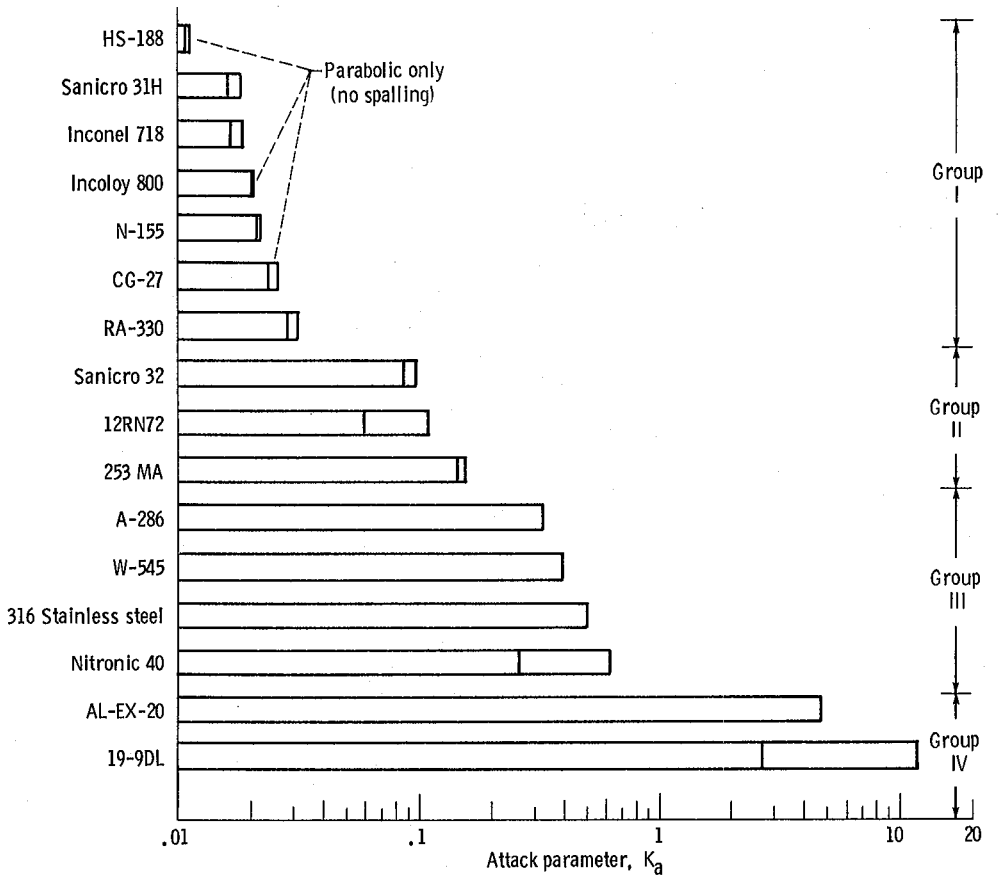

Figure 8. – Oxidation and corrosion attack parameter K_a for 3500-hr cyclic exposure in Stirling engine simulator rig. Temperature, 820° C; cycles length, 5 hr; $K_a = k_1^{1/2} + 10k_2$. (Duplicate samples.)

TABLE II. – GRAVIMETRIC AND THICKNESS CHANGE DATA FOR ALLOYS TESTED IN STIRLING ENGINE SIMULATOR MATERIALS TEST RIG FOR 3500 hr AT 820° C (5-hr CYCLES)

Group	Alloy	Weight change at 3524 hr, $\Delta W/A$, mg/cm^2	Thickness change (thickness measured from both sides), μm		Attack parameter[a], K_a
			Due to external scale	Due to internal depletion	
I	CG-27	1.425	14	44	0.028, 0.024
	Incoloy 800	1.135	21	64	0.023, 0.021
	HS-188	.72	---	56	0.011, 0.010
	N-155	.41	21	82	0.023, 0.022
	Inconel 718	.165	11	65	0.019, 0.017
II	RA-330	-.535	27	90	0.031, 0.029
	Sanicro 31H[b]	-1.19	18	158	0.018, 0.016
	Sanicro 32[b]	-1.36	22	224	0.098, 0.090
	12RN72[b]	-2.79	9	200	0.11, 0.06
	253 MA[b]	-5.97	4	76	0.16, 0.15
III	316 Stainless steel	-22.83	81	80	0.49, 0.48
	W-545	-33.23	43	296	0.42, 0.38
	A-286	-34.21	53	40	0.37, 0.37
	Nitronic 40	-41.75	133	56	0.66, 0.26
IV	19-9DL[c]	-86.05	802	(e)	12.49, 2.79
	AL-EX-20[d]	-215.59	724	(e)	4.68

[a]Duplicate samples.
[b]3675 hr.
[c]620 hr.
[d]825 hr.
[e]Not determined.

formed nearly pure Cr_2O_3 as either the most or secondmost intense oxide. The Cr_2O_3 oxide is listed as a sesquioxide, d (024) = 0.1818 nm in table III. Because Fe went into solution as Fe_2O_3, the value of d increased. As the d value approached 0.1839 nm, the oxide became essentially pure Fe_2O_3. Chromite spinel with a_o ranging from 0.835 to 0.840 nm also formed on most of the alloys during oxidation and corrosion testing. This chromite spinel appeared to be innocuous. Alloy A-286 showed another spinel with $a_o = 0.830$ nm along with a lower sesquioxide with $d = 0.1813$ nm, and also NiO was formed. Alloy 19-9DL, which oxidized catastrophically, formed as its two strongest oxides a spinel with $a_o = 0.840$ nm and the desirable oxide Cr_2O_3 with $d = 0.1821$ nm. This alloy may fail more for mechanical reasons than for lack of inherent oxidation resistance.

Metallography.—Photomicrographs of alloy specimens taken after the 3500-hr test are shown in figure 11. (Alloy photomicrographs are presented in order of change in weight as listed in table II.) Alloy CG-27 (fig. 11(a)) had an adherent oxide scale on the specimen surface. Incoloy 800 (fig. 11(b)) had a thin oxide scale over a depletion zone characterized by grain boundary oxide penetration and evidence of grain growth. Alloys HS-188, N-155, Inconel 718, and RA-330 (figs. 11(c) to (f), respectively) all had thin, adherent oxide scales with some depletion zones present in each alloy. Sanicro 31H (fig. 11(g)) had a thin oxide scale, but a fairly large depletion zone and grain boundary penetration of oxygen were also present. Sanicro 32 (fig. 11(h)) formed large voids in the depletion zone. A depletion zone of similar depth was evident in 12RN72 (fig. 11(i)). In contrast, 253 MA and 316 stainless steel (figs. 11(j) and (k), respectively) exhibited smaller depletion zones and evidence of oxide scale spalling. Severe grain boundary attack occurred in W-545 (fig. 11(l)) and resulted in almost total consumption of the alloy matrix beneath the surface oxide. Alloys A-286 and Nitronic 40 (figs. 11(m) and (n), respectively) both exhibited discontinuous oxide scales and a roughened surface resulting from preferential grain boundary attack. The final two alloys, 19-9DL and AL-EX-20 (figs. 11(o) and (p), respectively), were characterized by thin, discontinuous oxide scales. The oxide structures of these two alloys were not unexpected on the basis of their catastrophic oxidation behavior.

Electron microprobe analysis.—Six alloys (two each from groups I, II, and III) were selected for electron microprobe analysis because of their oxidation behavior

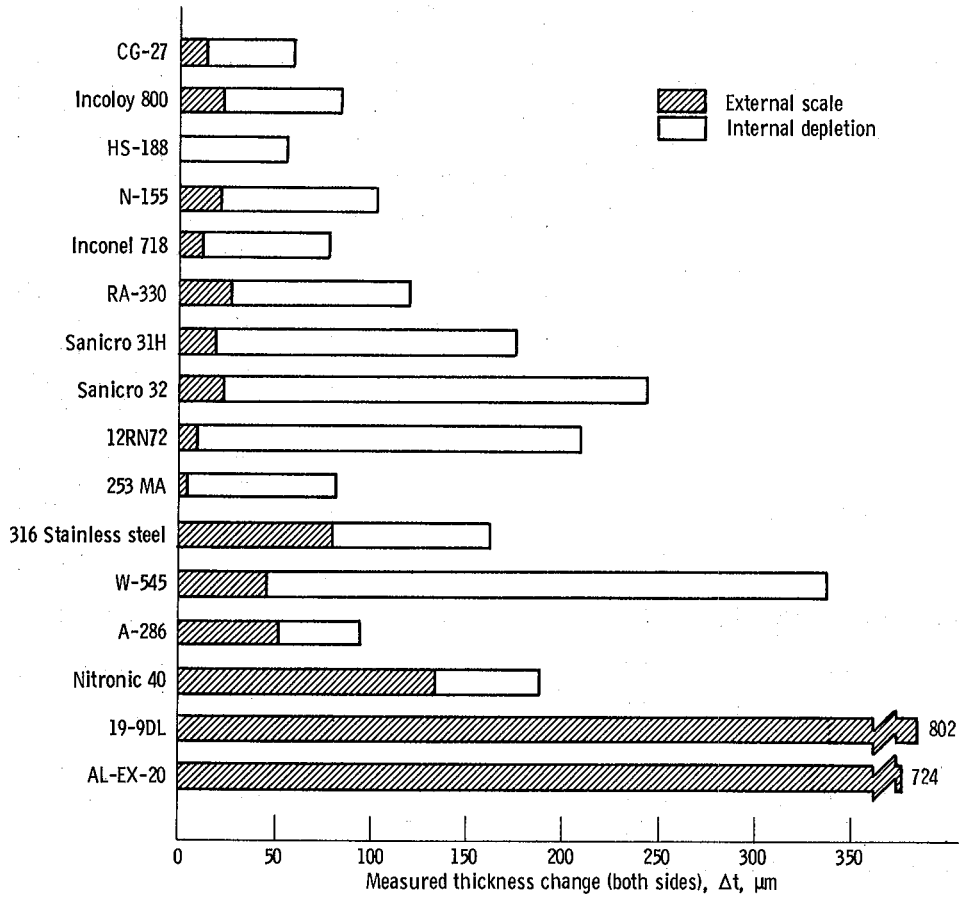

Figure 9. – Total thickness change of 16 alloys tested at 820° C for 3500 hr.

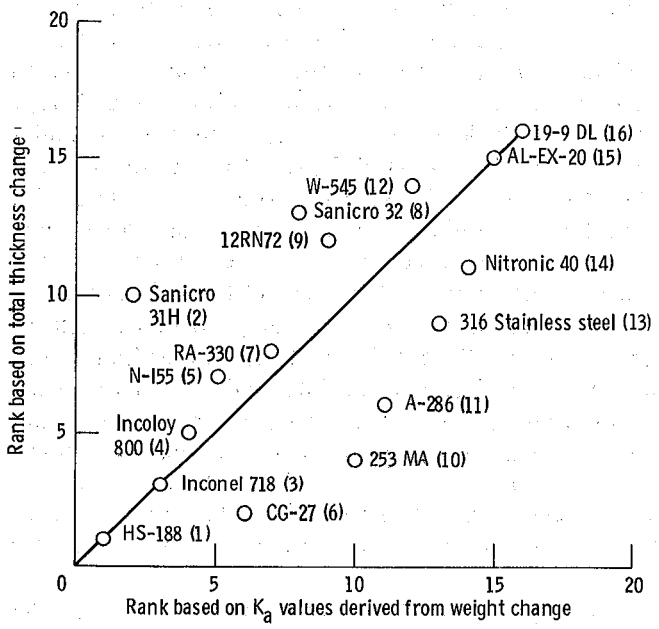

Figure 10. – Relationship of alloy oxidation rankings from total thickness change measurements and from attack parameter K_a estimates. Ranked from best rank (1) to worst rank (16). Results based on Stirling rig tests. Rank correlation coefficient, ρ, 0.691.

and resulting microstructures. Alloy CG-27, a group I alloy, was selected because it had excellent oxidation resistance and contained the least chromium of the 16 alloys tested in the rig. The distribution of the major alloying elements and oxygen in the oxide scale and the adjacent metal substrate of CG-27 (fig. 12) showed the surface oxide to be rich in iron, nickel, and to a lesser extent aluminum. Beneath this oxide layer was a thin, continuous oxide layer rich in chromium and titanium. Adjacent to the chromium-rich intermediate scale was an aluminum-rich oxide next to the metal substrate, which exhibited a wide zone of internally oxidized aluminum-rich, and somewhat fewer titanium-rich, protrusions.

A second group I alloy examined by electron microprobe was Incoloy 800. This alloy was selected because its microstructure (fig. 11(b)) indicated a significant depletion zone near the surface. The results (fig. 13) indicated this zone to be low in chromium and aluminum. A thin chromium-rich surface oxide and a metal substrate zone rich in aluminum beneath the oxide, similar to that observed for CG-27, apparently were responsible for the excellent oxidation resistance of this alloy. Iron, nickel, and titanium did not appear to be instrumental in the

TABLE III. – X-RAY DIFFRACTION DATA OF SPECIMEN SURFACE AFTER 3500-hr TEST IN ORDER OF DECREASING INTENSITY

[Values of d and a_o are in nanometers.]

Rank	Alloy	Chromium content, wt %	1	2	3	4
1	HS-188	22	0.1818 Sesquioxide	$a_o = 0.840$ Spinel	Mn_2O_3	0.408 (SiO_2)
2	Sanicro 31H	21	$a_o = 0.840$	0.1819	SiO_2	$(Mn_{0.983}Fe_{0.017})_2O_3$
3	Inconel 718	18	$a_o = 0.835$	0.1822	0.410(SiO_2)	----------
4	Incoloy 800	21	$a_o = 0.840$	0.1819	Mn_2O_3	0.409 (SiO_2)
5	N-155	21	$a_o = 0.840$	0.1826	0.411 (SiO_2)	0.272
6	CG-27	13	$a_o = 0.835$ } Spinel	0.1821 } Sesquioxide	0.1841 Sesquioxide	Trirutile, $d = 0.330$
7	RA-330	19	$a_o = 0.840$	0.1818	Mn_2O_3	----------
8	Sanicro 32	21	$a_o = 0.840$	0.1819	SiO_2	$(Mn_{0.983}Fe_{0.017})_2O_3$
9	12RN72	19	$a_o = 0.840$	0.1819	$(Mn_{0.983}Fe_{0.017})_2O_3$	SiO_2
10	253 MA	21	0.1839 Sesquioxide	$a_o = 0.835$ Spinel	SiO_2	0.1812 Sesquioxide
11	A-286	15	$a_o = 0.830$ Spinel	0.1813	NiO	----------
12	W-545	14	$a_o = 0.840$ Spinel	0.1849 } Sesquioxide	----------	----------
13	316 Stainless steel	18	0.1842 Sesquioxide	0.1824	$a_o = 0.845$ Spinel	Mn_2O_3
14	Nitronic 40	21	$a_o = 0.840$ Spinel	0.1843	----------	----------
15	AL-EX-20	5	0.1839 Sesquioxide	$a_o = 0.840$ Spinel	Mn_2O_3	----------
16	19-9DL	19	$a_o = 0.840$ Spinel	0.1821 Sesquioxide	0.1843 Sesquioxide	----------

oxidation of Incoloy 800, which contains much less titanium than CG-27.

Electron microprobe results for the group II alloy Sanicro 32 (fig. 14) indicated that oxygen had penetrated along grain boundaries to form primarily aluminum-rich oxides. Voids (fig. 11(h)) may contribute to the poorer oxidation resistance of this group II alloy. Note that the chromium-rich surface oxide was not uniform in thickness and that iron and nickel oxides had spalled from the surface. This may further account for the lower-ranking oxidation behavior of this alloy.

Electron microprobe results for the group II alloy 12RN72 (fig. 15) indicated deep oxygen penetration into the matrix of this alloy along grain boundaries. The oxide formed at the grain boundaries was rich in chromium and titanium. The alloy was also characterized by a nonuniform chromium-rich surface oxide layer containing iron. Spalling led to inferior oxidation resistance as compared with the group I alloys.

Metallographic results for the group III alloy W-545 (fig. 11(l)) indicated a large surface scale consisting of a porous oxide. Results from electron microprobe analyses (fig. 16) showed an outer oxide rich in iron, nickel, and chromium. Oxygen had penetrated uniformly into this alloy to a substantial depth. The oxide formed appeared to be rich in nickel with some chromium. Iron was depleted from this area, but discrete areas of molybdenum were observed near the surface. Aluminum and titanium did not appear to enter into the oxidation process of this alloy. The composition of W-545 is similar to that of CG-27 except for the large difference in aluminum content. This suggests that aluminum makes a major contribution to the oxidation resistance of CG-27 and that its low concentration in W-545 may explain the poor oxidation resistance of that alloy.

The poor oxidation resistance of A-286 can be attributed primarily to the discontinuous chromium-rich oxide shown in figure 17. Oxygen penetrated into the matrix, where some grain boundary oxides rich in aluminum and titanium formed.

Static-Air Cyclic Oxidation Tests

The standard NASA Lewis static-air-furnace cyclic oxidation tests (ref. 8) were conducted at 870° C for 200 hr. This temperature is 50 deg C above the proposed average use temperature anticipated for the automotive Stirling engine but corresponds to the maximum temperature anticipated in the engine. The 1-hr heating cycles presumably further accelerated the test as compared with the 5-hr cycles used in the Stirling simulator rig. The oxidation attack parameters K_a derived for the 18 alloys are plotted in figure 18. Ideally the relative alloy ranking in the accelerated cyclic static-air test should be the same as that in the Stirling cycle simulation test. Perfect correlation would follow the 45° line in the plot of cyclic static-air ranking versus Stirling simulation ranking (fig. 19). Here the actual ranking correlation coefficient ρ is 0.709. Statistically this is quite significant for 16 alloys (n = 16) (ref. 10). Therefore the risk in using the cyclic furnace test data to predict the best alloy results from the Stirling simulation rig is, in general, low. Good agreement was apparent except for alloys 12RN72 and 19-9DL. In any such approach 12RN72

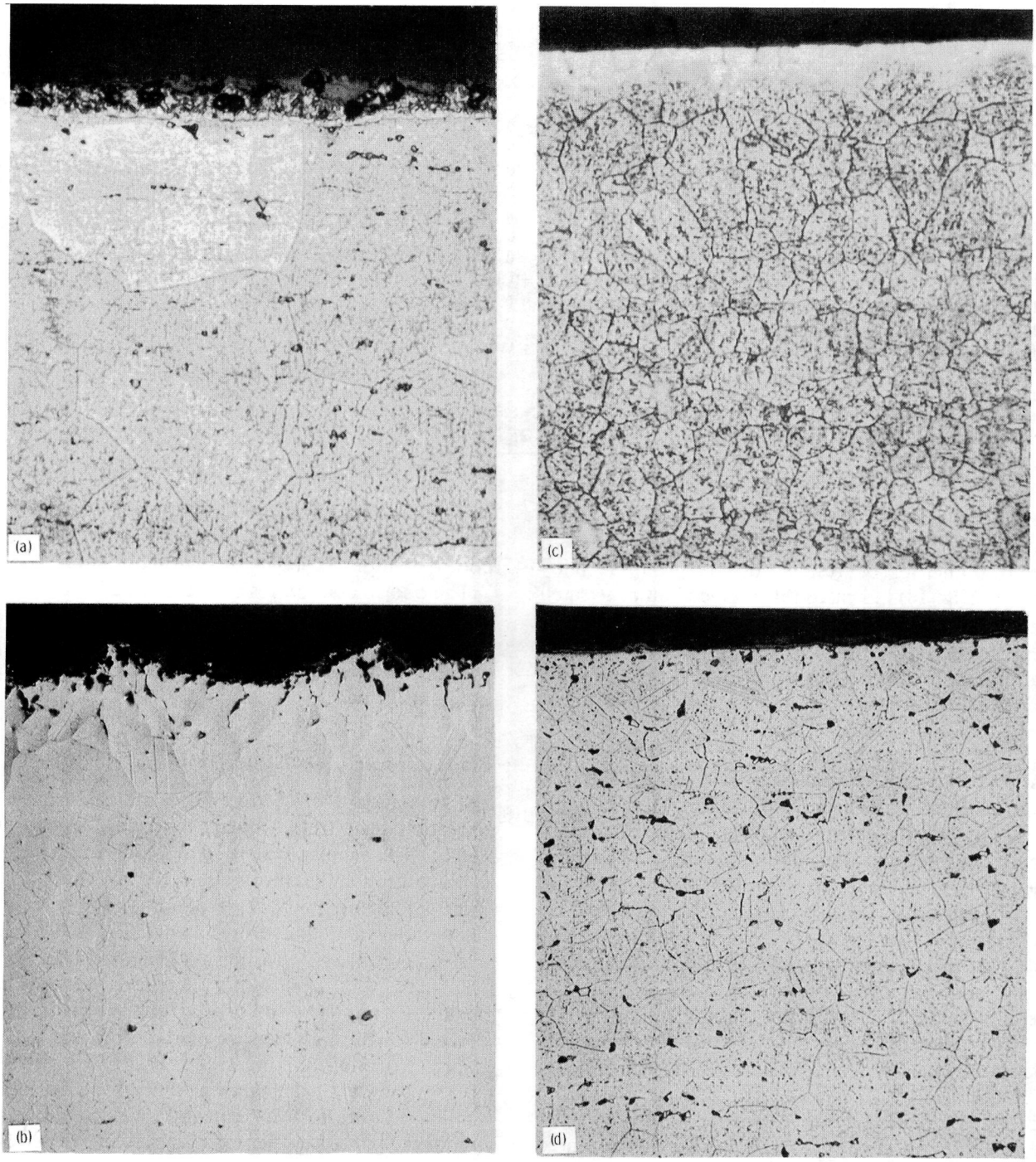

(a) CG-27.
(b) Incoloy 800.
(c) HS-188.
(d) N-155.

Figure 11. – Photomicrographs of 3500-hr oxidation and corrosion test specimens. Longitudinal view showing surface scales and depletion zones; magnification, 250.

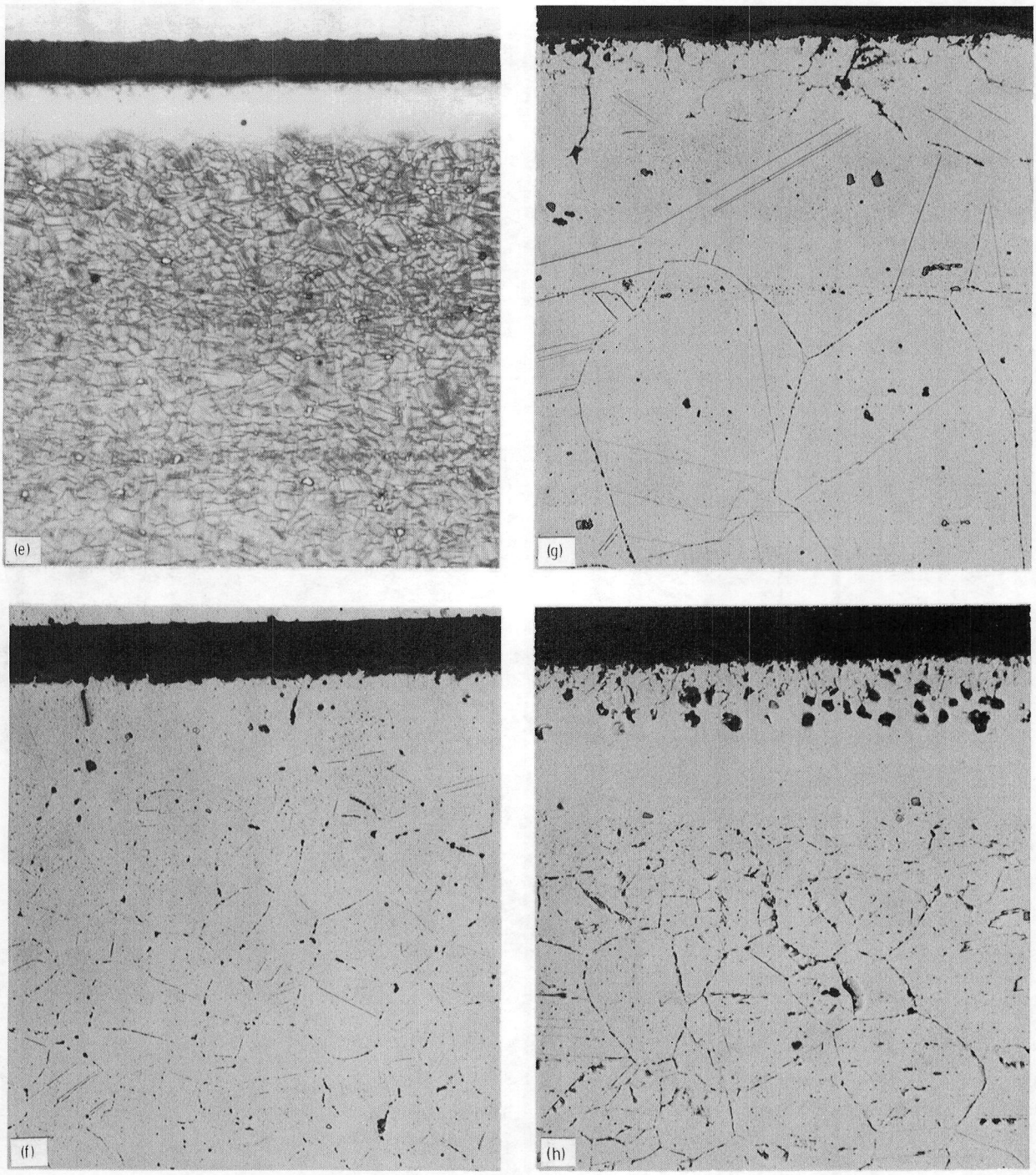

(e) Inconel 718.
(f) RA-330.
(g) Sanicro 31H.
(h) Sanicro 32.

Figure 11. – Continued.

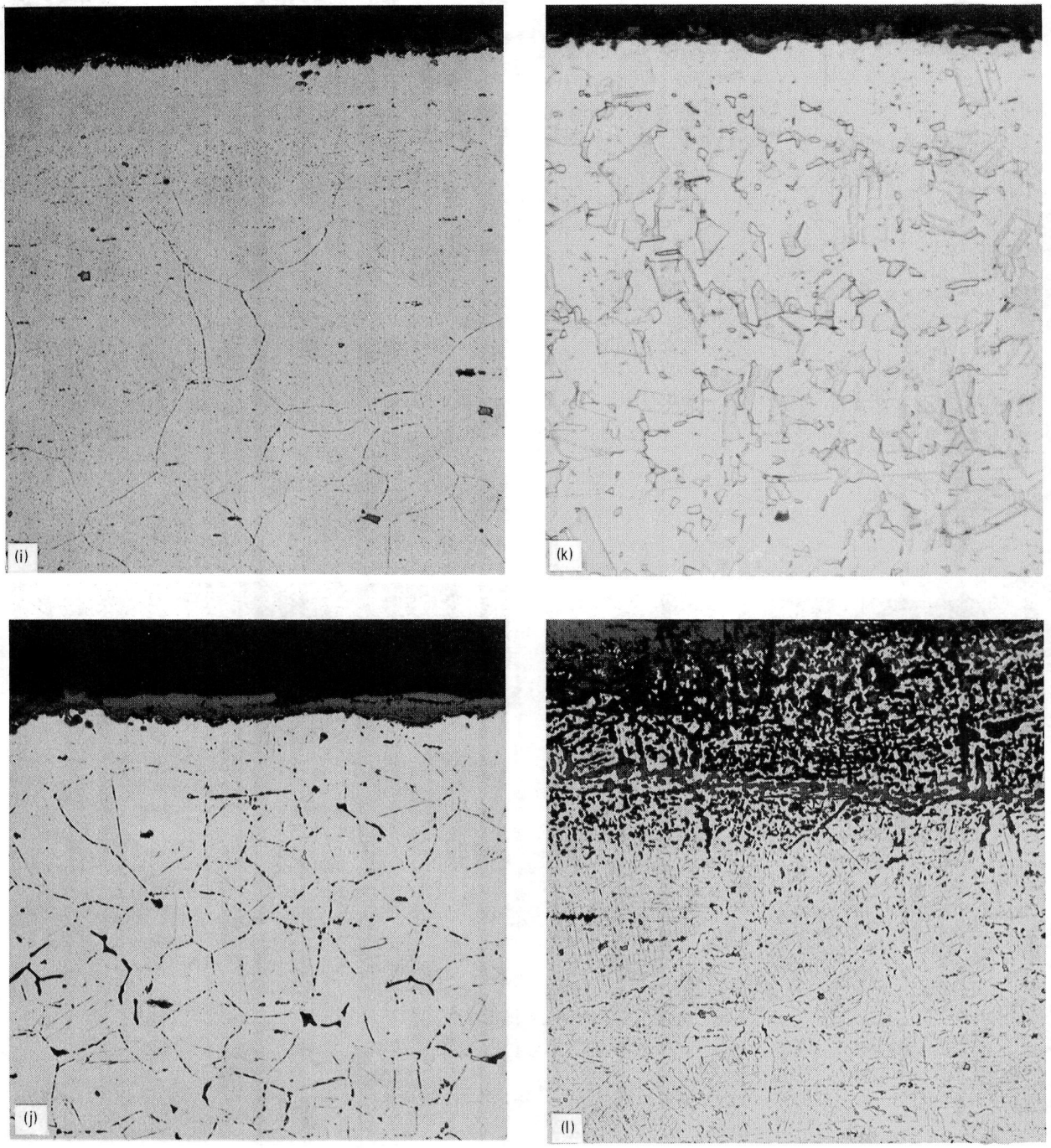

(i) 12RN72.
(j) 253 MA.
(k) 316 Stainless steel.
(l) W-545.

Figure 11. – Continued.

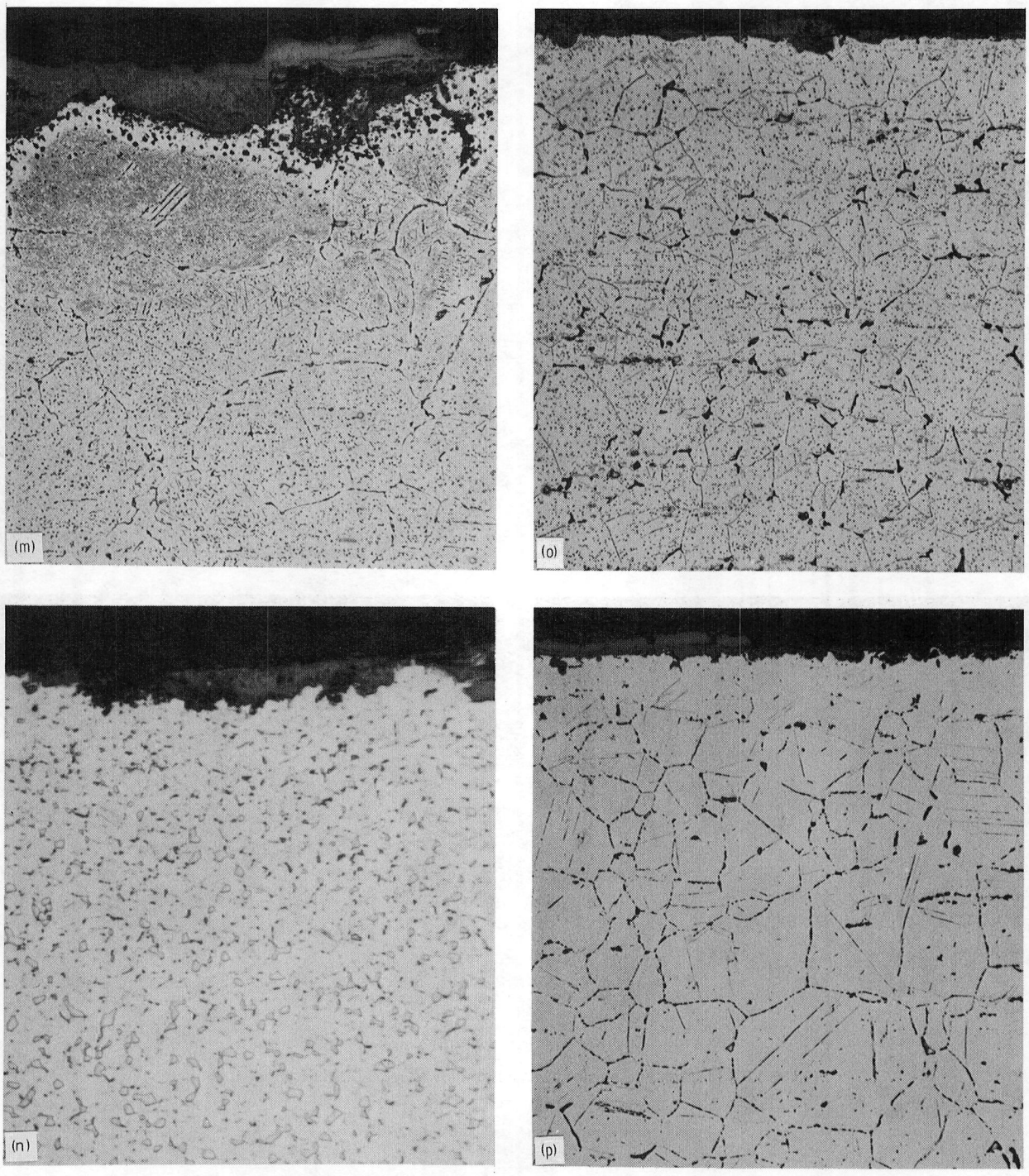

(m) A-286.
(n) Nitronic 40.
(o) 19-9DL.
(p) AL-EX-20.

Figure 11. – Concluded.

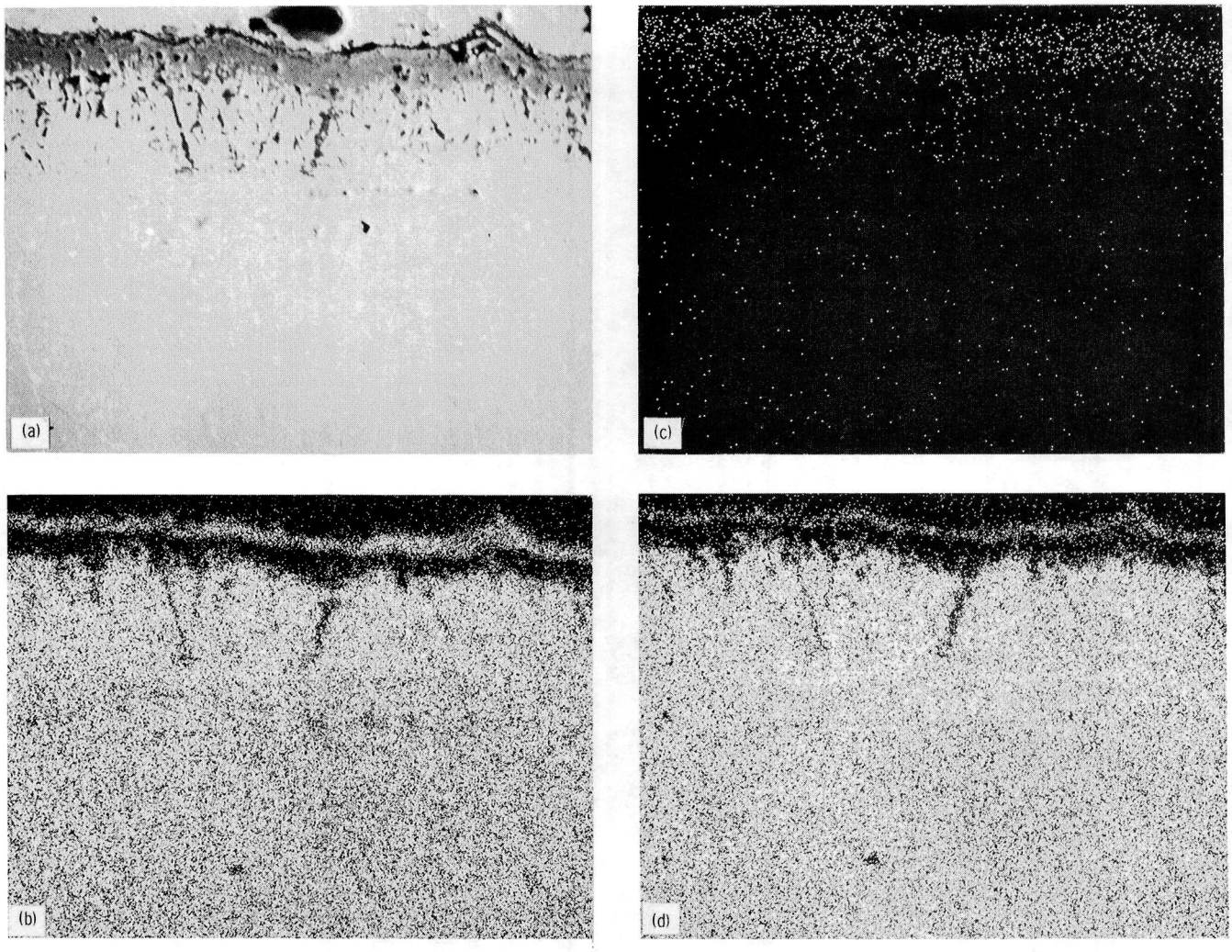

(a) BSE.
(b) Iron.
(c) Oxygen.
(d) Nickel

Figure 12. – Electron microprobe analyses of alloy CG-27. Magnification, 1000.

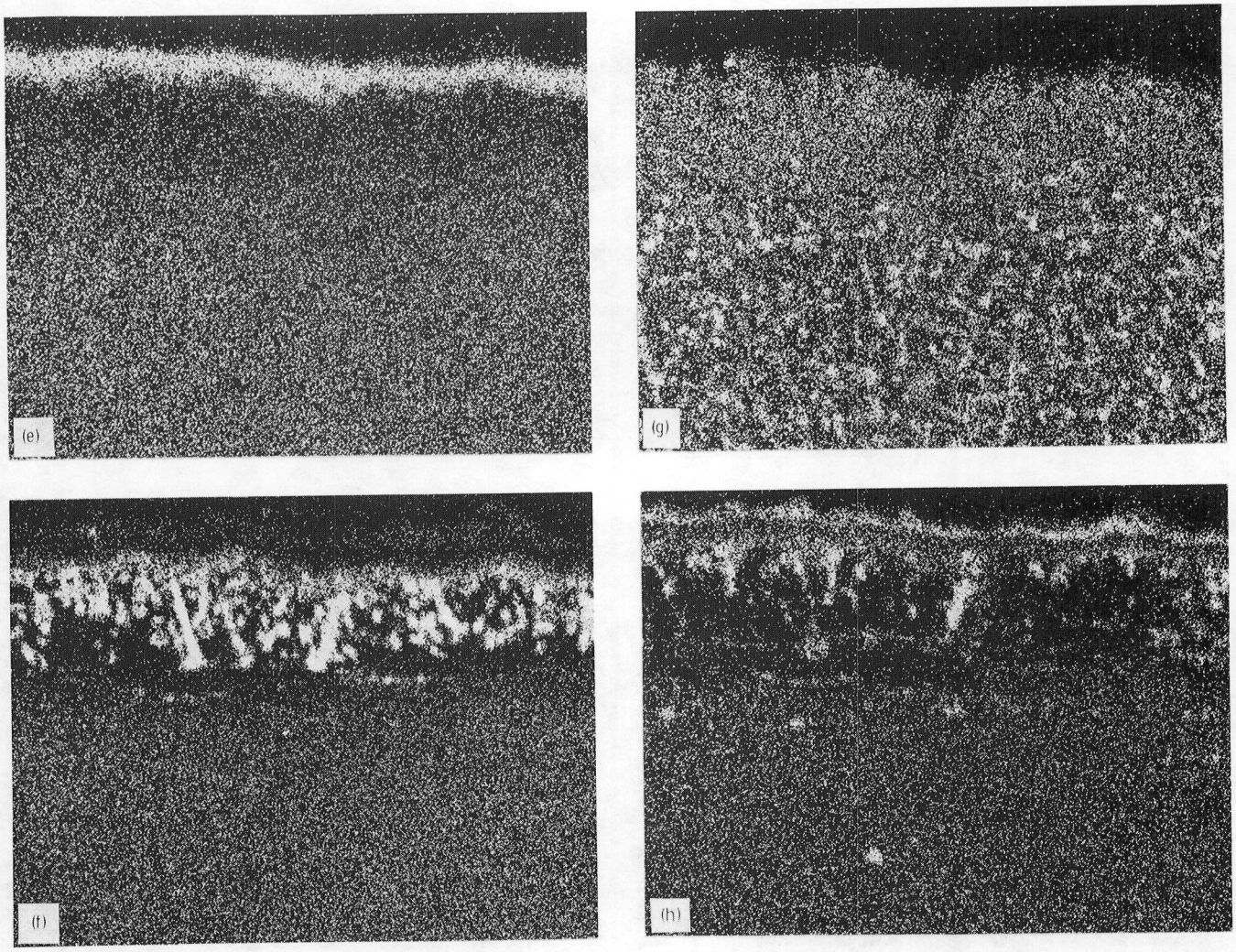

(e) Chromium.
(f) Aluminum.
(g) Molybdenum.
(h) Titanium.

Figure 12. – Concluded.

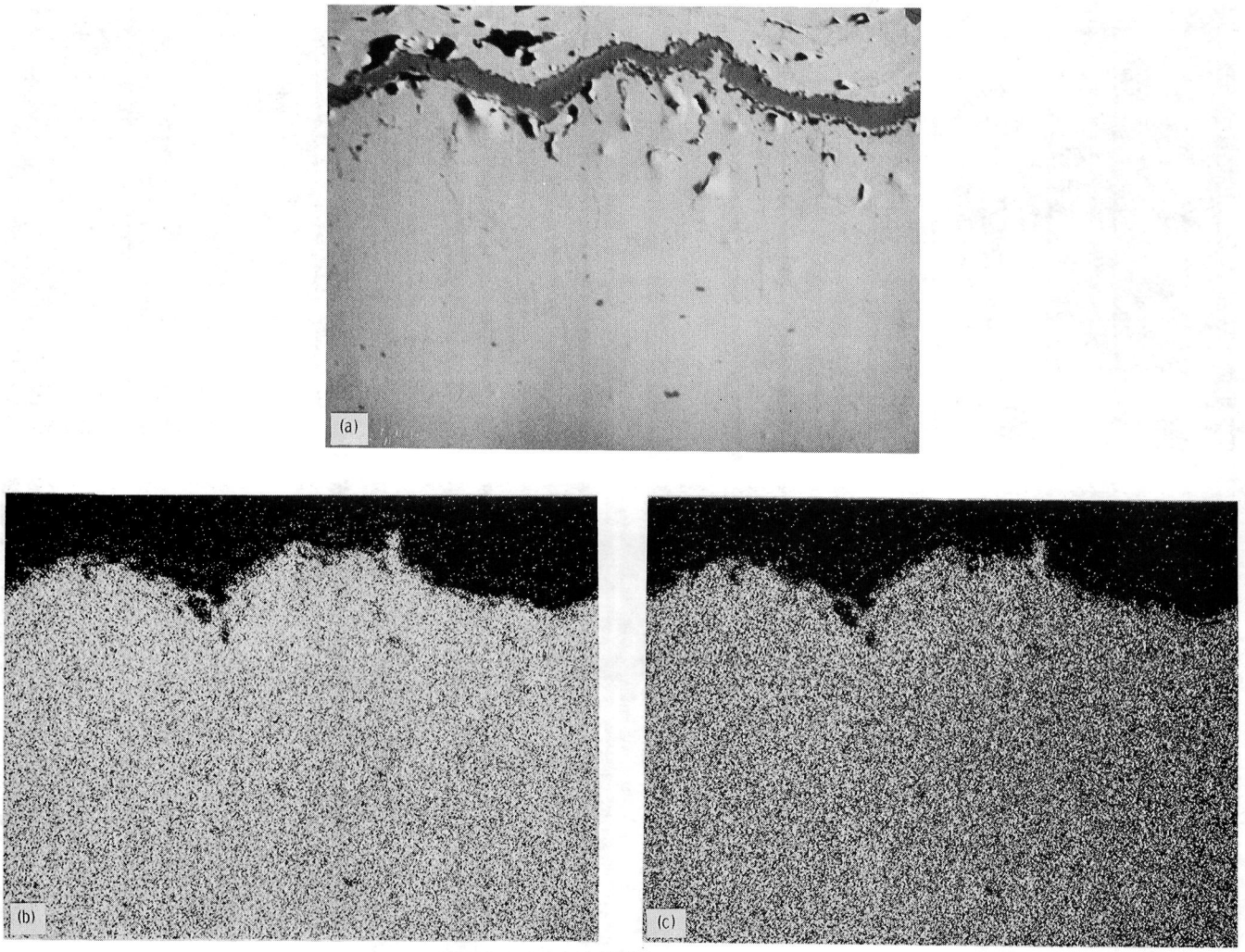

(a) BSE.
(b) Iron. (c) Nickel.

Figure 13. – Electron microprobe analyses of alloy Incoloy 800. Magnification, 500.

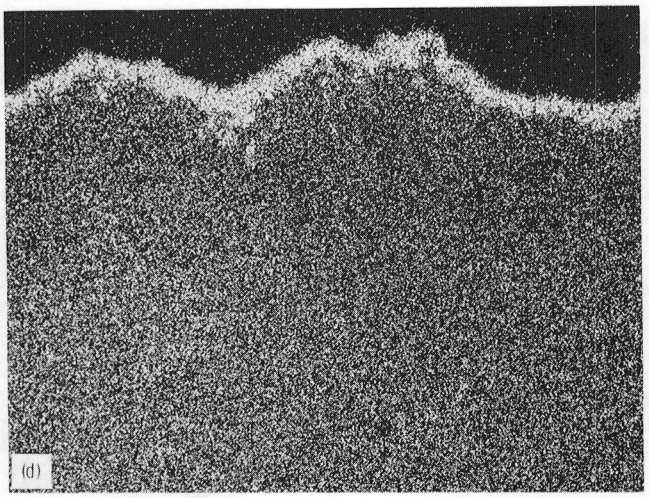

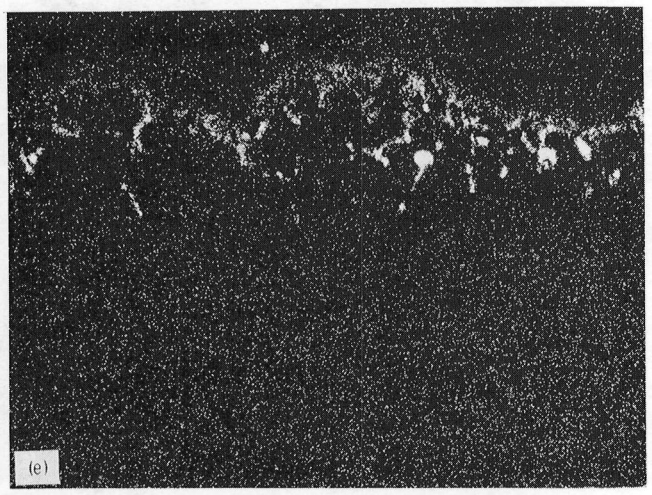

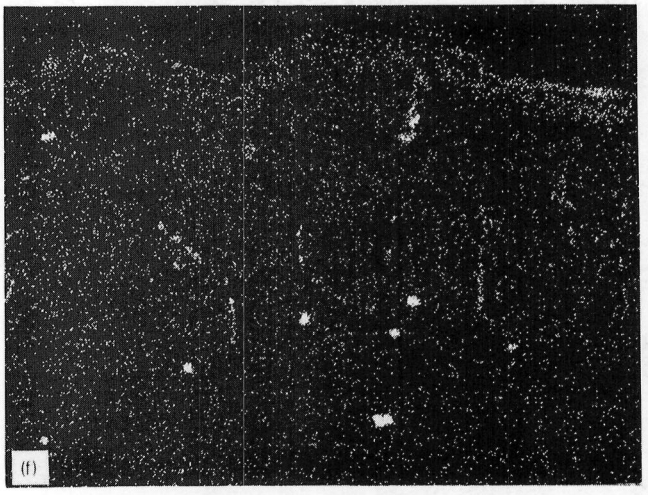

(d) Chromium.
(e) Aluminum. (f) Titanium.

Figure 13. – Concluded.

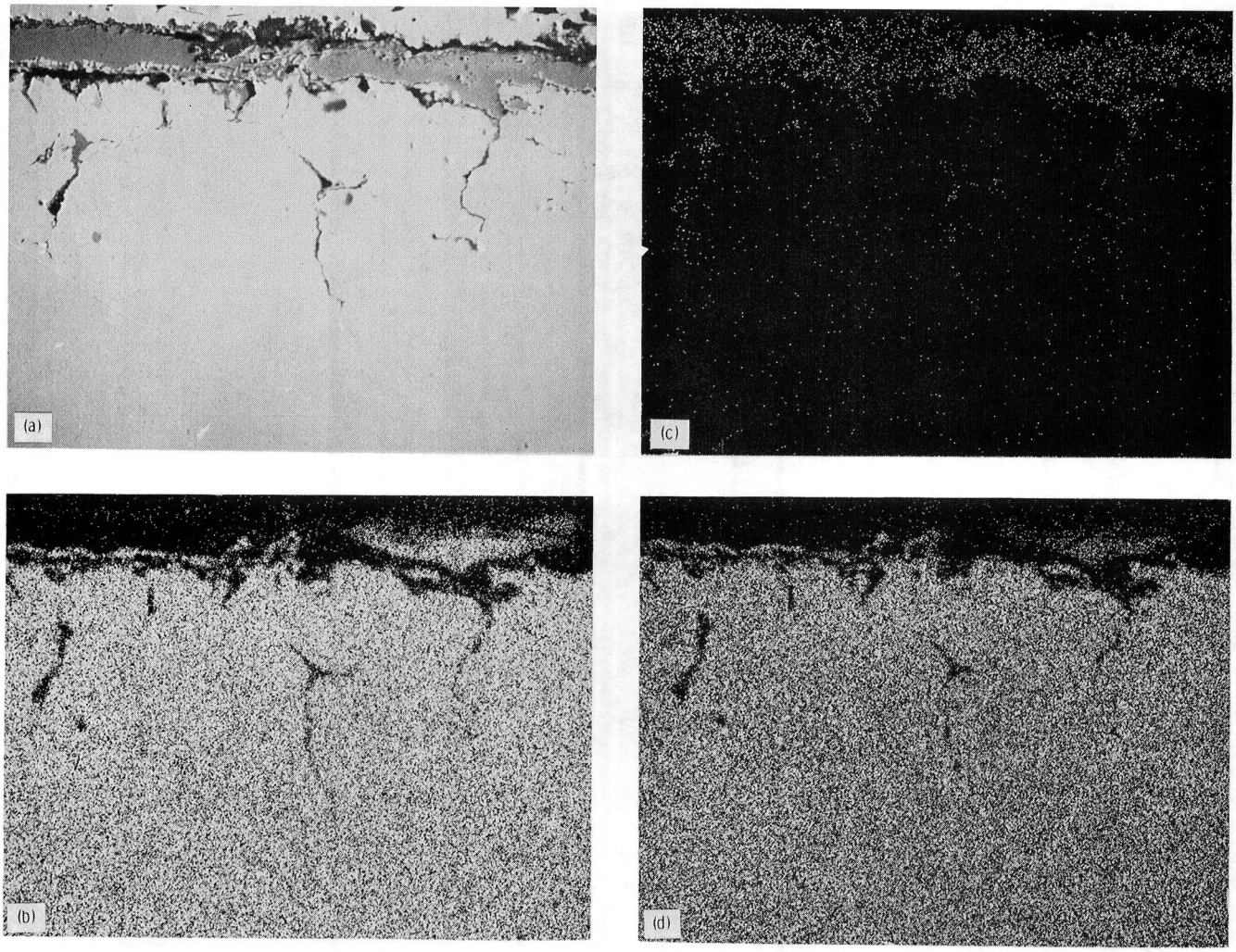

(a) BSE.
(b) Iron.
(c) Oxygen.
(d) Nickel.

Figure 14. – Electron microprobe analyses of alloy Sanicro 32. Magnification, 500.

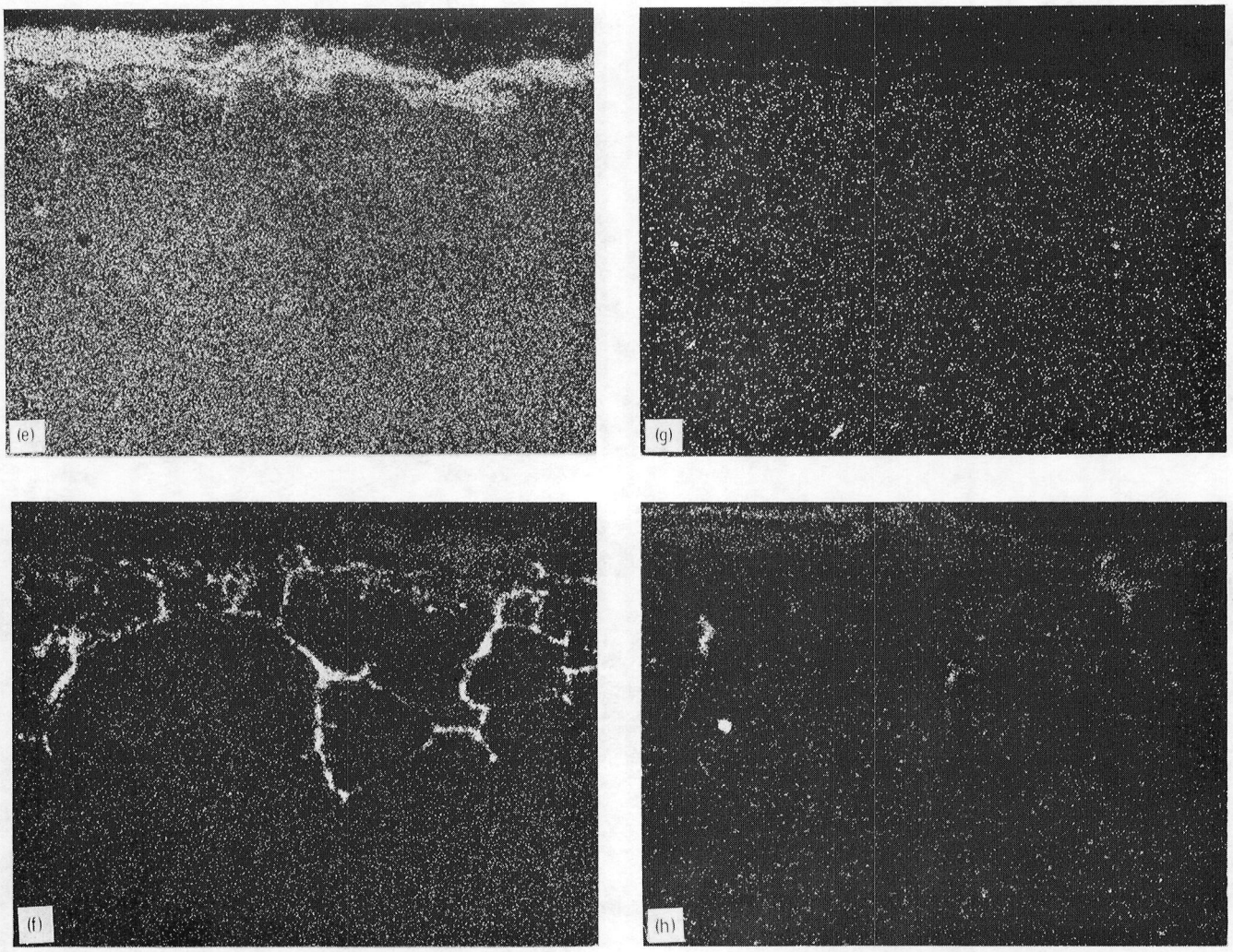

(e) Chromium.
(f) Aluminum.
(g) Titanium.
(h) Titanium.

Figure 14. – Concluded.

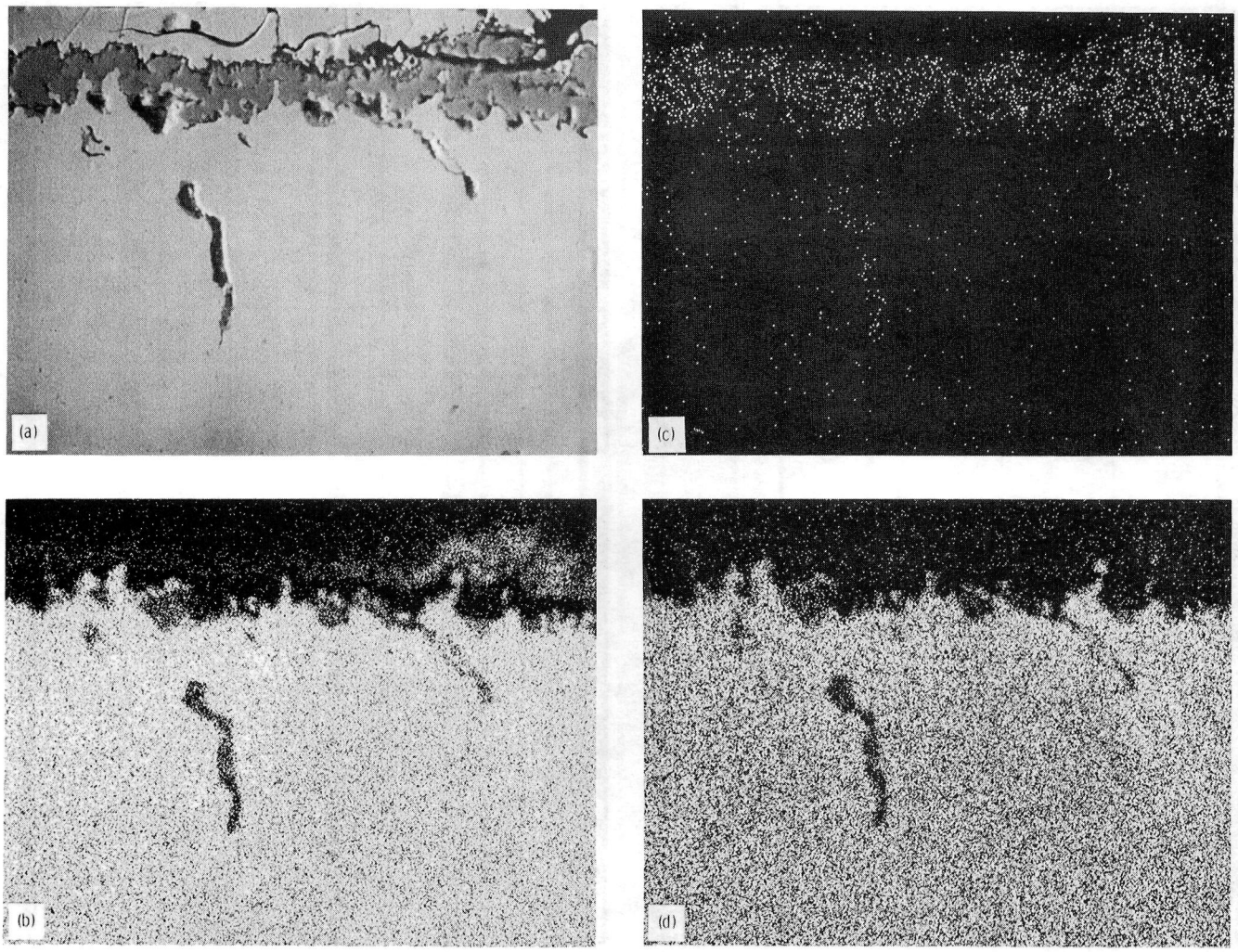

(a) BSE.
(b) Iron.
(c) Oxygen.
(d) Nickel.

Figure 15. – Electron microprobe analyses of alloy 12RN72. Magnification, 1000.

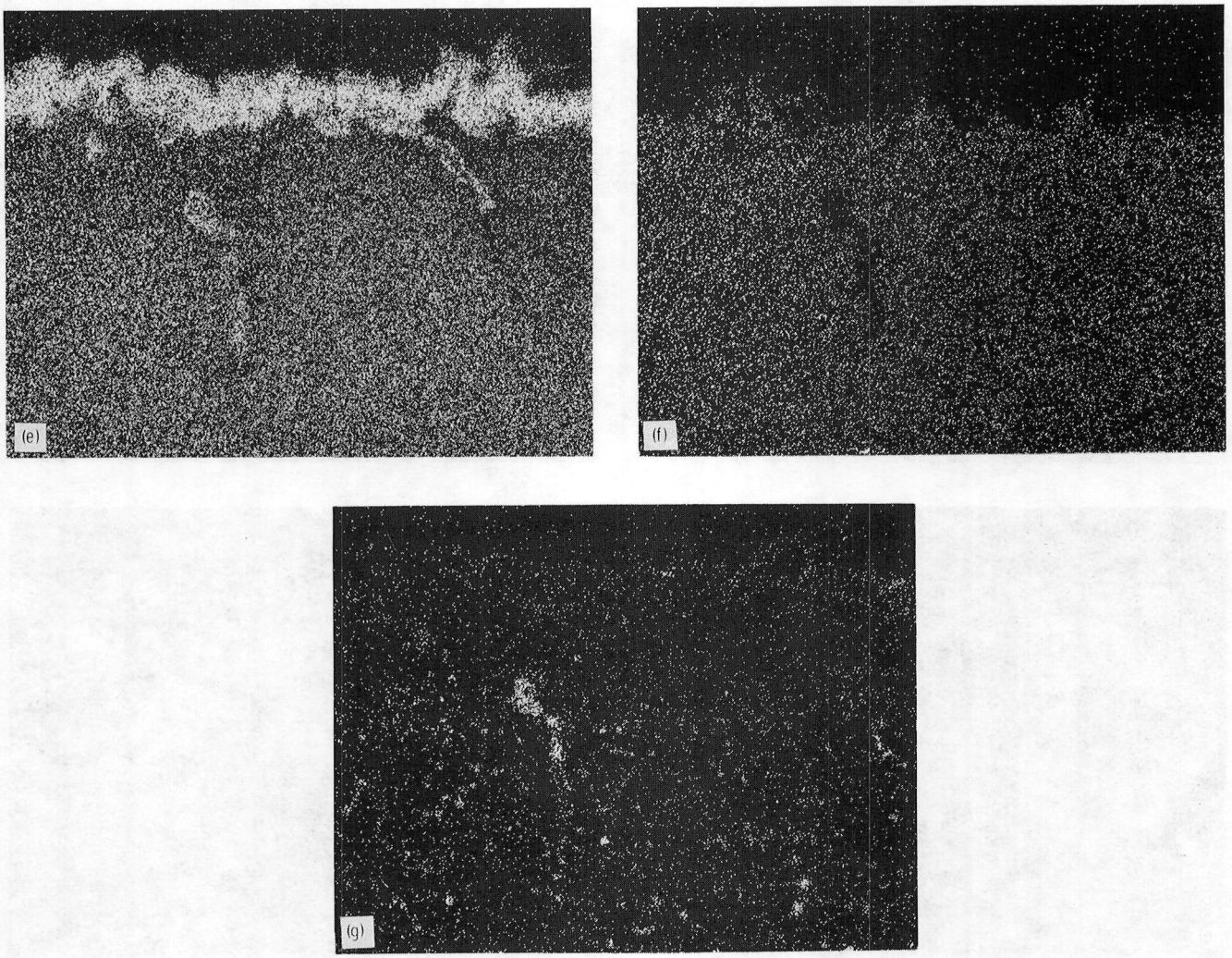

(e) Chromium.
(f) Molybdenum. (g) Titanium.

Figure 15. – Concluded.

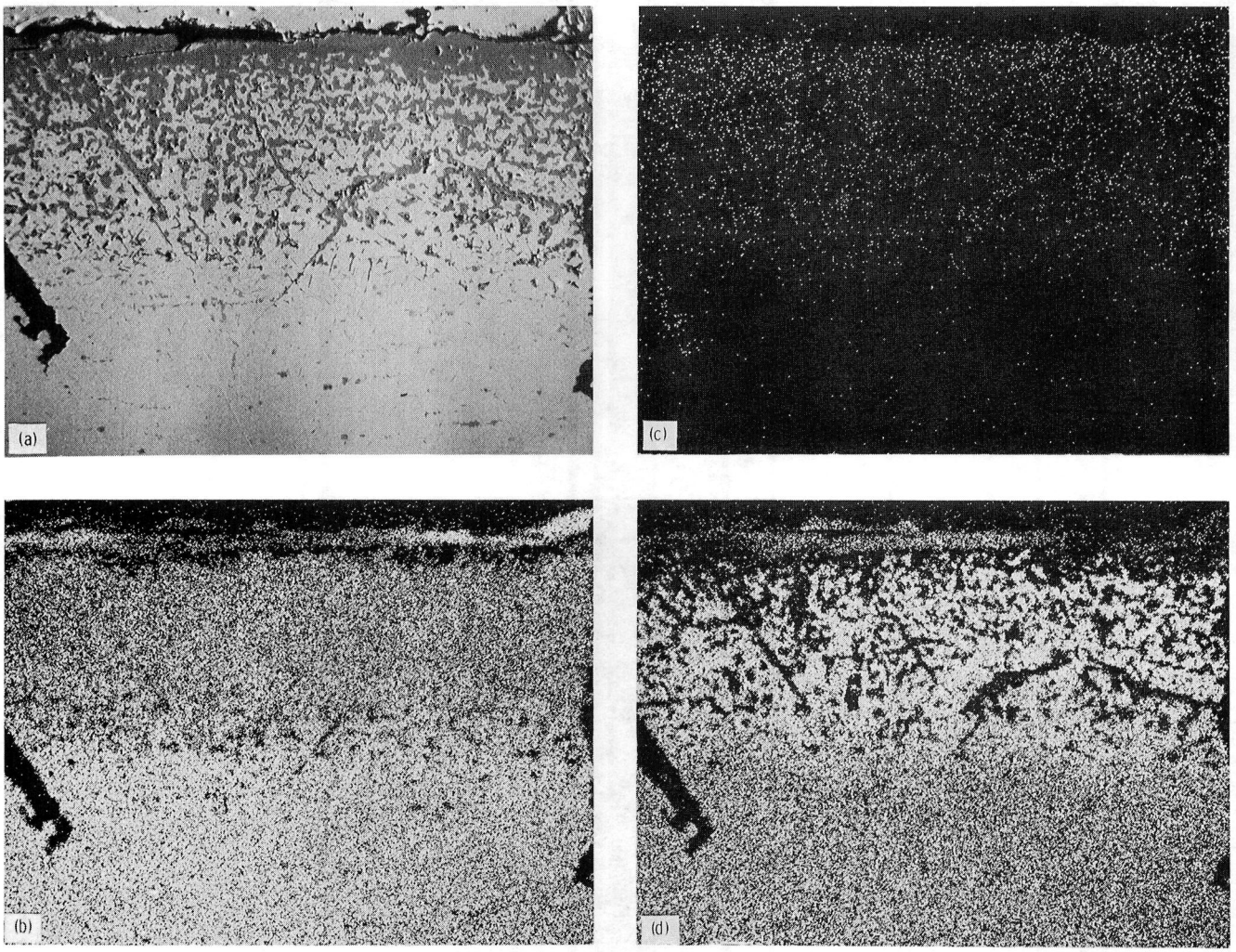

(a) BSE.
(b) Iron.
(c) Oxygen.
(d) Nickel.

Figure 16. – Electron microprobe analyses of alloy W-545. Magnification, 300.

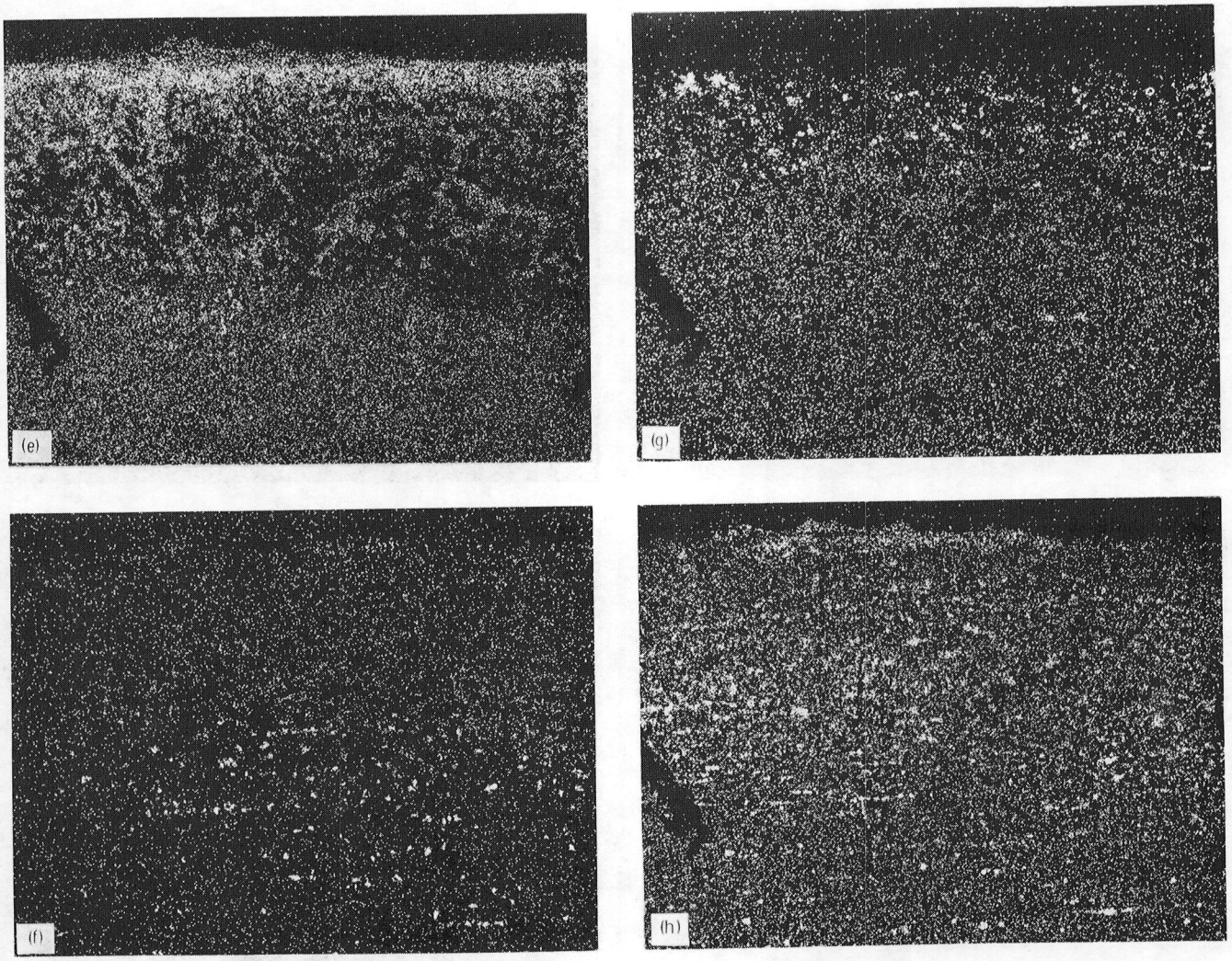

(e) Chromium.
(f) Aluminum.
(g) Molybdenum.
(h) Titanium.

Figure 16. – Concluded.

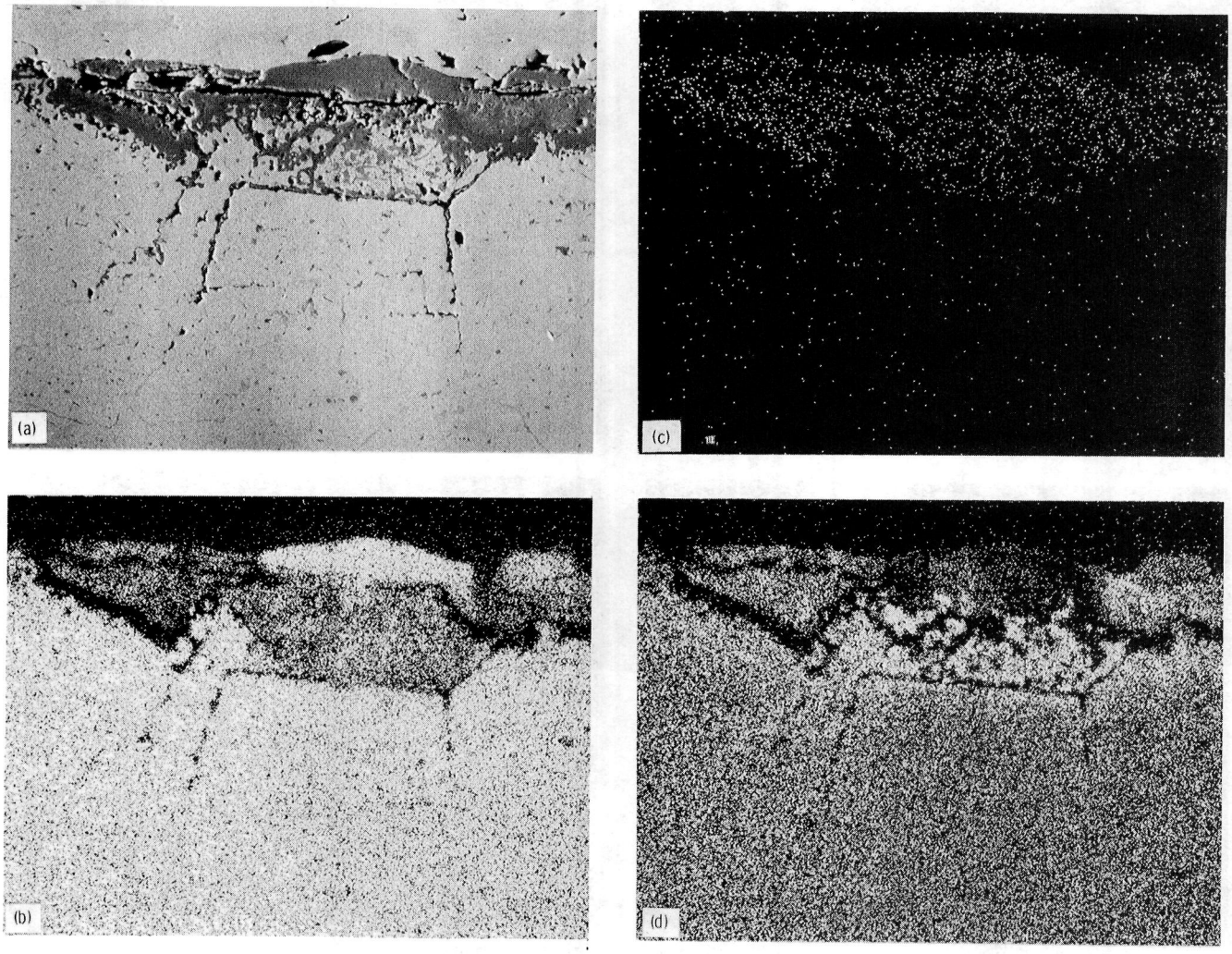

(a) BSE.
(b) Iron.
(c) Oxygen.
(d) Nickel.

Figure 17. – Electron microprobe analyses of alloy A–286. Magnification, 500.

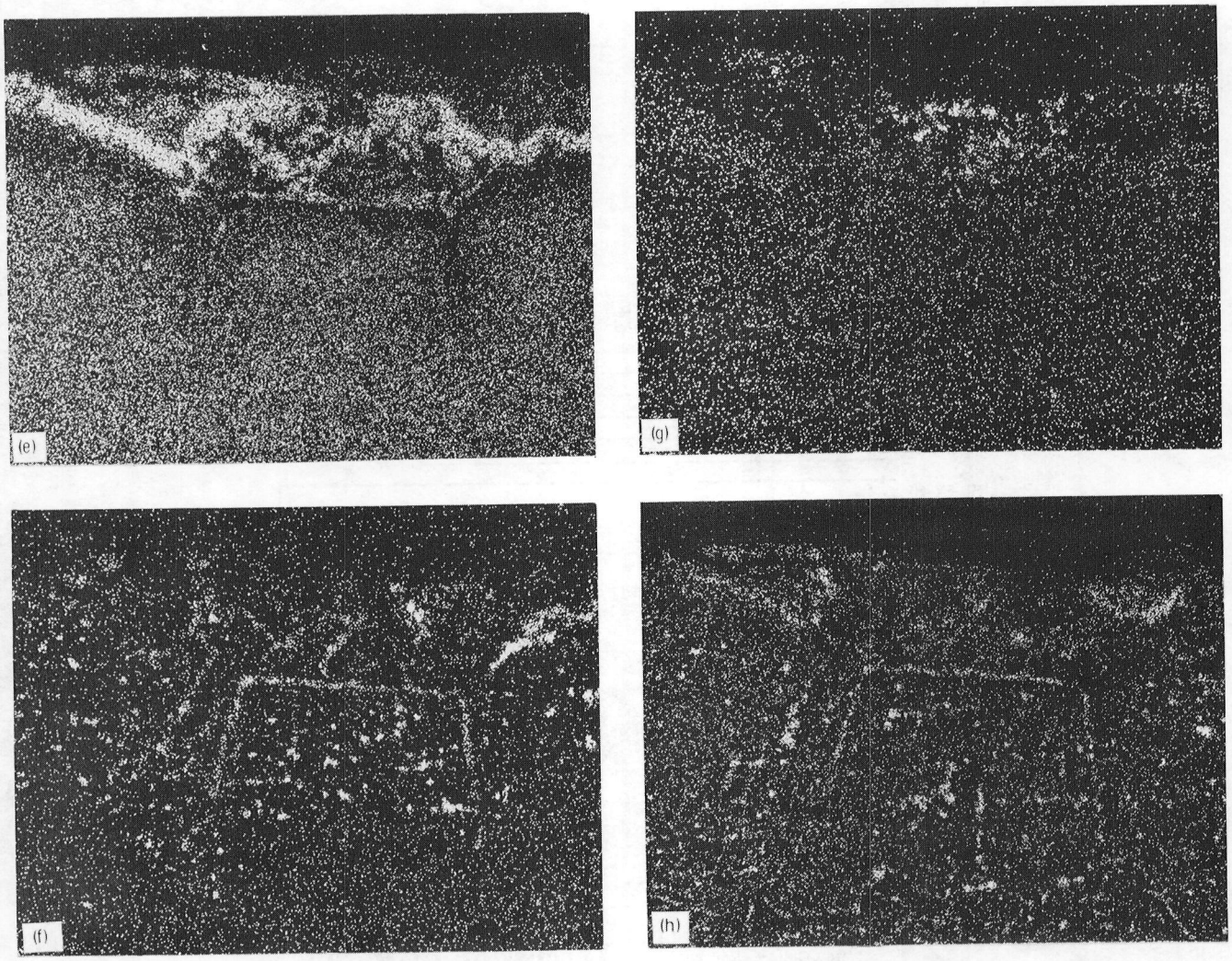

(e) Chromium.
(f) Aluminum.
(g) Molybdenum.
(h) Titanium.

Figure 17. – Concluded.

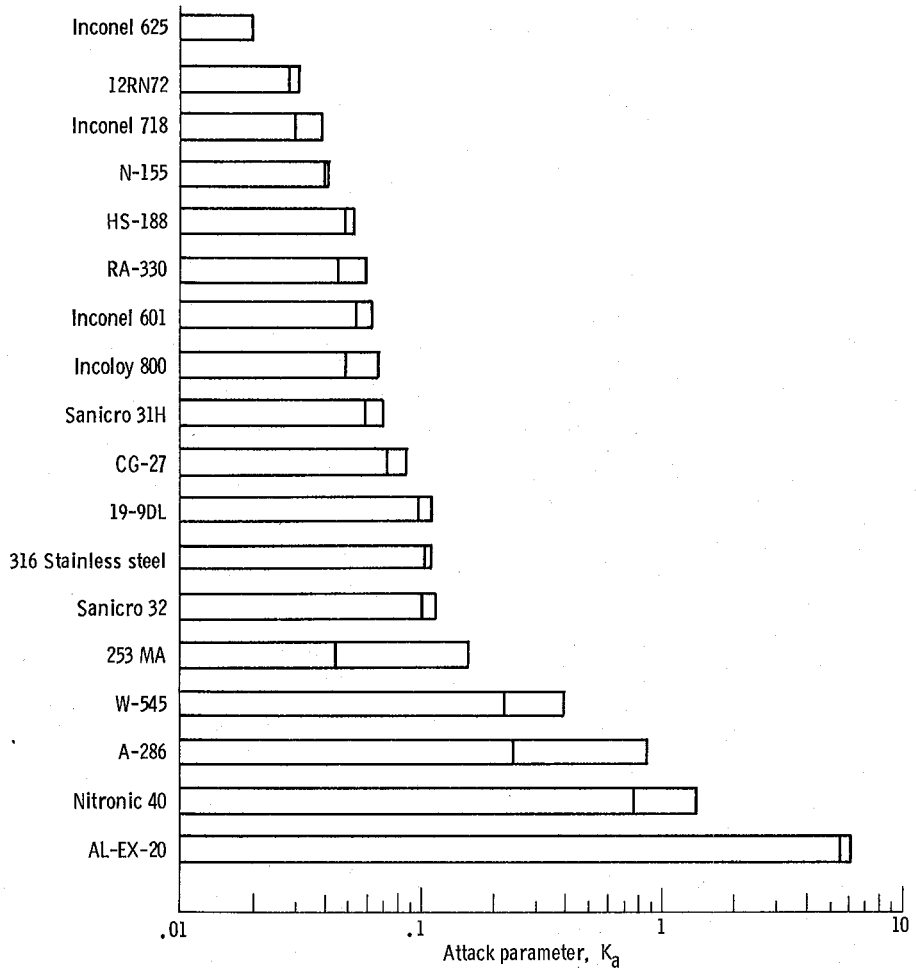

Figure 18. – Cyclic oxidation attack parameter K_a for 200-hr exposure in static air. Temperature, 870° C; 1-hr cycles. (Duplicate samples.)

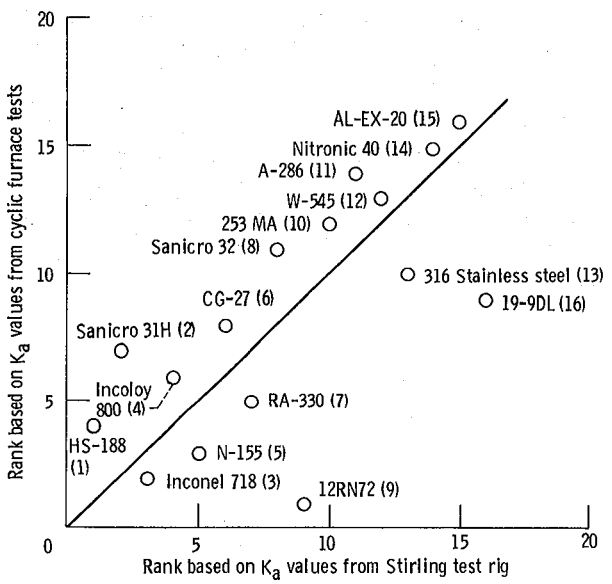

Figure 19. – Predictive relationship between alloy oxidation rankings K_a derived from cyclic furnace tests (200 1-hr cycles at 870° C) and from 3500-hr Stirling materials simulator rig tests. Rank correlation coefficent, ρ, 0.709.

would probably be included in any second-round evaluation. However, since CG-27 was midway in this cyclic furnace evaluation, it might well have been missed if the screening cutoff criteria were too strict. This shows the advantage of closer test simulation if the test time penalty is not too great.

Discussion of Results

Some insight into the excellent oxidation and corrosion behavior of CG-27 along with other group I alloys can be gained from the electron microprobe results presented in figures 12 to 17. The chromium distribution in the six alloys shows that group I alloys CG-27 and Incoloy 800 had a chromium-rich oxide layer ranging in thickness from about 3 to 4 μm. The poorer oxidation behavior of group II and III alloys was characterized by chromium-rich oxide layers about 8 μm thick (group II alloys) and from 20 to 35 μm thick (group III alloys). All 16 alloys studied herein formed Cr_2O_3 chromite spinels as their major oxides. The thin, adherent oxide formed by the

group I alloys CG-27 and Incoloy 800 is believed to be a major contributor to the oxidation resistance of these alloys.

Further comparison of the six alloys characterized by electron microprobe techniques indicated that iron and nickel were present as a thin outer oxide in group I alloys. In contrast, in group II alloys and especially in group III alloys, iron and nickel were observed as thick, discrete areas of oxide that were in some cases ready to spall from the specimen. Evidently in group I alloys the iron and nickel oxides formed early in the 3500-hr test, and then oxide formation of the more reactive alloying elements took over the oxidizing process. The thicker oxides and higher spalling rates in particular for group III alloys (specific weight losses of 23 to 42 mg/cm^2 as compared with little or no weight loss for group I alloys) suggest that iron and nickel oxides formed throughout the 3500-hr test.

Particular interest was focused on the apparent roles of the more reactive oxide-forming alloying elements aluminum and titanium contained in some of the alloys. In CG-27 internal oxidation of aluminum to a depth of approximately 10 μm below the oxide-metal interface was evident. In addition, aluminum was present in the surface oxide, and an argument can be made that a thin oxide layer rich in aluminum existed adjacent to the metal substrate. A similar, though not as evident, distribution of aluminum occurred in Incoloy 800, the second group I alloy examined in the electron microprobe. Incoloy 800 contains 0.38 wt % aluminum as compared with 1.5 wt % in CG-27. A thin, discontinuous aluminum-rich oxide layer near the oxide-metal interface and grain boundary oxides were previously noted for Sanicro 32. Titanium, at a concentration of 2.5 wt % in CG-27, appeared to be associated with aluminum in the oxide scales and as internally oxidized. In contrast, for the group III alloy W-545, which contains slightly more titanium (2.85 wt %) but much less aluminum (0.2 wt %), titanium does not preferentially oxidize.

The role of reactive elements such as yttrium, scandium, cerium, zirconium, and hafnium in improving oxide scale adherence particularly for Fe-Cr-Al, Ni-Cr-Al, and Co-Cr-Al alloys has been investigated in much detail (refs. 11 to 16). The standard free energies of oxide formation of these reactive elements are more negative than those for iron, nickel, cobalt, chromium, and aluminum. Small additions (<1 at. %) of these elements have been shown to dramatically improve oxide scale adherence and to reduce spalling in cyclic oxidation. The exact mechanism by which such an improvement occurs is not agreed upon by investigators in this field. For example, yttrium and scandium have been reported to increase oxide growth rates by forming rapid diffusion paths along yttria and scandia stringers (ref. 11). Increased grain boundary transport of oxygen has been demonstrated by ^{18}O tracer studies on Ni-Cr-Al alloys with zirconium additions (ref. 17). The resulting oxide adherence has been attributed (refs. 11, 12, and 15) to (1) mechanical oxide pegging; (2) stress-strain accommodations at the oxide-matrix interface; (3) increased chemical bonding across the interface; and (4) a vacancy sink mechanism that precludes void formation at the oxide-metal interface, which would promote spalling.

It is postulated that for the alloys studied herein, aluminum plays a role similar to that of the reactive elements discussed previously. Aluminum has a more negative standard free energy of oxide formation than do the major alloying constituents of the candidate heater-head-tube alloys such as iron, nickel, and chromium. The internal aluminum oxidation suggests that controlling the inward oxygen diffusion plays a major role in the oxidation of CG-27 and probably Incoloy 800. Although the remaining group I alloys were not studied by electron microprobe techniques, the reactive elements niobium in N-155, niobium and aluminum in Inconel 718, and lanthanum in HS-188 probably play a role similar to that of aluminum in the two alloys that were examined. The results further suggest that although 0.4 wt % aluminum is adequate to be effective in promoting good scale adherence (Incoloy 800, Sanicro 32, Sanicro 31H, and Inconel 718), a concentration of 0.2 wt % aluminum such as exists for W-545 and A-286 is insufficient to improve the oxidation behavior of these alloys. It is not clear from this study which of the previously suggested models for oxide scale adherence is to be preferred.

Concluding Remarks

On the basis of the analysis of the oxidation weight change data and X-ray, metallographic, and electron microprobe analyses of tested specimens groups I and II, comprising 10 alloys, had excellent or good oxidation resistance and these alloys are potential candidates for heater-head-tube application in the automotive Stirling engine. These 10 alloys can be further ranked, however, on the basis of other considerations such as strength, resistance to hydrogen permeation, cost (cobalt or nickel base), and strategic metal (primarily cobalt) content. The 10 best oxidation-resistant alloys (groups I and II alloys) were ranked (table IV), taking into consideration these other factors, which have been determined in other programs conducted at the NASA Lewis Research Center (refs. 2 to 7). Alloy CG-27 was given top priority, as indicated in table IV. This alloy has been chosen as the leading candidate alloy for future builds of prototype automotive Stirling engines. United Stirling AB is continuing to test tubes of CG-27, Sanicro 32, 12RN72, Sanicro 31H, and Inconel 625 in a P-40 Stirling engine to gain comparative engine experience on these five alloys.

Alloy CG-27 oxidized by pure parabolic oxidation over the 3500-hr engine simulation rig test. The resulting

TABLE IV. – RANKING OF TEN BEST OXIDATION-RESISTANT STIRLING ENGINE HEATER-HEAD-TUBE ALLOYS

Alloy	Priority	Comments
CG-27	1	Best overall oxidation resistance, strength, and resistance to H_2 permeation
Sanicro 32	2	Low cost, but lower strength
12RN72	3	Low cost, but lower strength
Inconel 718	4	Nickel-base alloy—will drive cost up. (Inconel 625 and 601 from fig. 18 also fall into this category.)
Sanicro 31H	5	Probably will not meet the required strength at 820° C for 3500-hr operation
Incoloy 800	6	
RA-330	7	
253 MA	8	
N-155	9	Cobalt content precludes use
HS-188	10	Cobalt content precludes use

oxide attack parameter, $K_a = 0.026$, quantitatively characterized the oxidation behavior of this alloy and, from prior cyclic oxidation experience, CG-27 was considered to have excellent oxidation resistance. Furthermore the alloy offers good resistance to hydrogen permeation (ref. 7), has greater strength at the proposed engine operating temperature than the currently used alloy N-155, contains a relatively low concentration of the strategic metal chromium (13 percent as compared with 20 percent in N-155), contains no cobalt (as compared with 20 percent in N-155), and should be readily fabricable into heater head tubes. The lower cost Sanicro 32 and 12RN72 alloys still appear attractive, but their strength capabilities at the high operating temperatures of current designs for the automotive Stirling engine are in serious doubt.

Summary of Results

The oxidation and corrosion behavior of 16 candidate Stirling engine heater-head-tube alloys tested at 820° C for 3500 hr in a diesel-fuel-fired Stirling simulator materials test rig is summarized as follows:

1. Alloy CG-27, an iron-nickel base superalloy, showed excellent resistance to the combustion environment, characterized by a low value of the attack parameter, $K_a = 0.026$.

2. The reactive elements aluminum and probably titanium along with chromium played a major role in the oxidation and corrosion resistance of CG-27. A thin, adherent, chromium-rich inner oxide scale and a subsurface aluminum-rich scale adjacent to the metal along with internal aluminum oxidation led to the excellent oxidation behavior of CG-27.

3. Nine other alloys were judged to have excellent or good oxidation and corrosion resistance on the basis of K_a values and specific weight change data. However, the high cobalt content, low strength, and high initial cost (of the cobalt and nickel alloys) eliminated all but two of these alloys, Sanicro 32 and 12RN72, from consideration for automotive applications.

4. Six of the 16 alloys exhibited poor or catastrophic resistance to the combustion environment.

5. Alloys that form oxide scales rich in iron or nickel exhibited poor oxidation resistance.

6. A 200-hr-exposure accelerated cyclic oxidation test (1-hr heating cycles) in general gave relative rankings for each alloy similar to those given by the Stirling simulation rig, except that the attractive alloy CG-27 might have been eliminated because of its middle ranking.

National Aeronautics and Space Administration
Lewis Research Center
Cleveland, Ohio, March 27, 1984

References

1. Brogan, J. J.: Highway Vehicle Systems Program Overview. Highway Vehicle Systems Contractor's Coordination Meeting. CONF-771037, 1978, pp. 3-5.
2. Witzke, W. R.; and Stephens, J. R.: Creep-Rupture Behavior of Seven Iron-Base Alloys After Long Term Aging at 760° C in Low Pressure Hydrogen. NASA TM-81534, 1980.
3. Miscencik, J. A.: Evaluation of Candidate Stirling Engine Heater Tube Alloys for 1000 Hours at 760° C. NASA TM-81578, 1980.
4. Stephens, J. R.: Hostile Environmental Conditions Facing Candidate Alloys for the Automotive Stirling Engine. NASA TM-82632, 1981.
5. Schuon, S. R.; and Miscencik, J. A.: Effect of Oxide Films on Hydrogen Permeability of Candidate Stirling Engine Heater Head Tube Alloys. NASA TM-82824, 1982.
6. Miscencik, J. A.: Evaluation of Candidate Stirling Engine Heater Tube Alloys at 820° C and 860° C. NASA TM-82837, 1982.
7. Stephens, J. R.; Cronin, M. T.; and Skog, E.: Stirling Engine Materials Research at NASA Lewis, MTI, and USAB. Proceedings of the Twentieth Automotive Technology Development, Contractors Coordination Meeting, P-120, Society of Automotive Engineers, Inc., Apr., 1983, pp. 103-113.
8. Barrett, C. A.; and Lowell, C. E.: High Temperature Cyclic Oxdiation Furnace Testing at NASA Lewis Research Center. J. Test. Eval., vol. 10, no. 6, Nov., 1982, pp. 273-278.
9. Barrett, C. A.; Miner, R. V.; and Hull, D. R.: The Effects of Cr, Al, Ti, Mo, W, To, and Cb on the Cyclic Oxidation Behavior of Cast Ni-Base Superalloys at 1100° and 1150° C, submitted to Oxidation of Metals, 1983.
10. Conover, W. J.: Practical Nonparametric Statistics, Second ed., John Wiley, 1980.

11. Tien, J. K.; and Pettit, F. S.: Mechanism of Oxide Adherence on Fe-25Cr-4Al (Y or SC) Alloys. Metall. Trans., vol. 3, June, 1972, pp. 1587–1599.
12. Allam, I. M; Whittle, D. P.; and Stringer, J.: Improvements in Oxidation Resistance by Dispersed Oxide Addition: Al_2O_3-Forming Alloys. Oxid.Met., vol. 13, no. 4, Aug., 1979, pp. 381–401.
13. Smialek, J. L.: Discussion Section The Relationship Between Oxide Grain Morphology and Growth Mechanisms for Fe-Cr-Al and Fe-Cr-Al-Y Alloys. by J. Electrochem, Soc., vol. 126, no. 12, Dec., 1979, pp. 2275–2276.
14. Khan, A. S.; Lowell, C. E.; and Barrett, C. A.: The Effect of Zirconium on the Isothermal Oxidation of Nominal Ni–14Cr–24Al Alloys. J. Electrochem. Soc., vol. 27, no. 3, Mar., 1980, pp. 670–679.
15. Barrett, C. A.; Khan, A. S.; and Lowell, C. E.: The Effect of Zirconium on the Cyclic Oxidation of NiCrAl Alloys. J. Electrochem. Soc., vol. 128, no. 1, Jan., 1981, pp. 25–32.
16. Reddy, K. P. R.; Smialek, J. L.; and Cooper, A. R.: ^{18}O Tracer Studies of Al_2O_3 Scale Formation on NiCrAl Alloys. Oxid. Met., vol. 17, nos. 5/6, June, 1982, pp. 429–449.

1. Report No.	2. Government Accession No.	3. Recipient's Catalog No.
NASA TM-83609		

4. Title and Subtitle	5. Report Date
Oxidation and Corrosion Resistance of Candidate Stirling Engine Heater-Head-Tube Alloys	May 1984
	6. Performing Organization Code 778-35-03

7. Author(s)	8. Performing Organization Report No.
Joseph R. Stephens and Charles A. Barrett	E-2028
	10. Work Unit No.

9. Performing Organization Name and Address	11. Contract or Grant No.
National Aeronautics and Space Administration Lewis Research Center Cleveland, Ohio 44135	
	13. Type of Report and Period Covered Technical Memorandum

12. Sponsoring Agency Name and Address	14. Sponsoring Agency ~~Code~~ Report No.
U.S. Department of Energy Office of Vehicle and Engine R&D Washington, D.C. 20545	DOE/NASA/51040-53

15. Supplementary Notes

Final report. Prepared under Interagency Agreement DE-AI01-77CS51040.

16. Abstract

Sixteen candidate iron-base Stirling engine heater-head-tube alloys were evaluated in a diesel-fuel-fired simulator materials test rig to determine their oxidation and corrosion resistance. Sheet specimens were tested at 820° C for 3500 hr in 5-hr heating cycles. Specific weight change data and an attack parameter K_a were used to categorize the alloys into four groups; 10 alloys had excellent or good oxidation and corrosion resistance and six alloys had poor or catastrophic resistance. Metallographic, X-ray, and electron microprobe analyses aided in further characterizing the oxidation and corrosion behavior of the alloys. Alloy compositions, expecially the reactive elements aluminum, titanium, and chromium, played a major role in the excellent oxidation and corrosion behavior of the alloys. The best oxidation resistance was associated with the formation of an iron-nickel-aluminum outer oxide scale, an intermediate oxide scale rich in chromium and titanium, and an alumium-rich oxide scale adjacent to the metallic substrate, which exhibited a zone of internal oxidation of aluminum and to some extent titanium.

17. Key Words (Suggested by Author(s))	18. Distribution Statement
Stirling engine, Oxidation, Corrosion, Tube alloys	Unclassified - unlimited STAR Category 26 DOE Category UC-96

19. Security Classif. (of this report)	20. Security Classif. (of this page)	21. No. of pages	22. Price*
Unclassified	Unclassified	31	A03

*For sale by the National Technical Information Service, Springfield, Virginia 22161

NASA-Langley, 1984

National Aeronautics and
Space Administration

Washington, D.C.
20546

Official Business
Penalty for Private Use, $300

THIRD-CLASS BULK RATE

Postage and Fees Paid
National Aeronautics and
Space Administration
NASA-451

NASA

POSTMASTER: If Undeliverable (Section 158 Postal Manual) Do Not Return